



CHALMERS
UNIVERSITY OF TECHNOLOGY

Activated carbon from biomass waste as potential materials for uranium removal

Downloaded from: <https://research.chalmers.se>, 2025-06-16 18:17 UTC

Citation for the original published paper (version of record):

Giraldo, L., Serafin, J., Dziejarski, B. et al (2025). Activated carbon from biomass waste as potential materials for uranium removal. *Chemical Engineering Science*, 306.
<http://dx.doi.org/10.1016/j.ces.2025.121222>

N.B. When citing this work, cite the original published paper.



Activated carbon from biomass waste as potential materials for uranium removal

Liliana Giraldo^a, Jarosław Serafin^{b,c,*}, Bartosz Dziejarski^{d,e,f},
Juan Carlos Moreno-Piraján^{b,*}

^a Facultad de Ciencias, Departamento de Química, Grupo de Investigación en Calorimetría, Universidad Nacional de Colombia, Bogotá, Colombia

^b Facultad de Ciencias, Departamento de Química, Grupo de Investigación en Sólidos Porosos y Calorimetría, Universidad de los Andes, Bogotá, Colombia

^c Department of Inorganic and Organic Chemistry, University of Barcelona, Martí i Franquès, 1-11, 08028 Barcelona, Spain

^d Department of Chemistry and Chemical Engineering, Division of Energy and Materials, Chalmers University of Technology, SE-412 96 Gothenburg, Sweden

^e Department of Space, Earth and Environment, Division of Energy Technology, Chalmers University of Technology, SE-412 96 Gothenburg, Sweden

^f Faculty of Environmental Engineering, Wrocław University of Science and Technology, 50-370 Wrocław, Poland

ARTICLE INFO

Keywords:

Calorimetry
Kinetic and Thermodynamic
PSD
Biomass
Separation Uranium
Adsorption

ABSTRACT

This study investigates the synthesis and characterization of two nitrogen-doped activated carbons derived from corn cobs for the removal of uranium (VI) ions from aqueous solutions. The materials were characterized using a range of techniques, including thermogravimetric analysis (TGA), Fourier-transform infrared spectroscopy (FTIR), scanning electron microscopy (SEM), and nitrogen adsorption isotherms. Particle size distribution (PSD) was determined through immersion calorimetry, and adsorption performance was evaluated using the Langmuir, Freundlich, and Sips isotherm models. Among these, the Sips model provided the best fit, with maximum adsorption capacities of 51.66, 46.32, and 22.12 mg/g for CCAKN7, CCAK7, and CC, respectively, at 298 K. Adsorption kinetics followed a pseudo-second-order model, reaching equilibrium within 55 min, indicating rapid adsorption. Thermodynamic analysis revealed that the adsorption process was spontaneous and exothermic, with a negative Gibbs free energy and enthalpy change, confirming the feasibility of uranium adsorption. Furthermore, the study demonstrated that nitrogen doping enhances the surface functionality of the activated carbons, significantly improving their uranium uptake compared to unmodified materials. These findings suggest that nitrogen-doped activated carbons from corn cobs are promising candidates for the efficient removal of uranium (VI) from contaminated water sources, contributing to sustainable nuclear waste management.

1. Introduction

The ever-increasing global energy demand, fueled by rapid economic growth and industrialization, has spurred intensive exploration of alternative energy sources that prioritize safety, efficiency, environmental harmony, and cleanliness. These alternatives are poised to supplant conventional fossil fuels like oil, derivatives, and coal. Notably, nuclear energy is progressively assuming a central role worldwide, aiming to replace the traditional fuels that have been both extensively consumed and detrimental to the environment.

While nuclear energy's adoption has raised debates, careful application and stringent safety measures can establish it as a viable energy source, contributing to mitigating ecological and environmental challenges such as global warming associated with fossil fuel use (Corner

et al., 2011; Lei et al., 2023; Fan et al., 2021; Dong et al., 2018; Wang et al., 2019). It's imperative to acknowledge that the advancement of nuclear energy also brings about increased nuclear safety risks. Past nuclear accidents underscore the need for rigorous management, especially in preventing the release of radioactive waste due to various human activities like spent fuel disposal, mineral processing, nuclear weapon production, and medical, industrial, and research applications of radionuclides (Burns et al., 2012; Huang et al., 2018; Spirin et al., 2015; Schulte-Herbrüggen et al., 2016).

In nations with operational nuclear power plants, the secure disposal of radioactive waste emerges as a pressing global concern due to its profound impact on ecosystems and the potential threat to life forms. Among the most hazardous byproducts from nuclear facilities is uranium, a highly abundant element with potent radioactivity, long half-

* Corresponding authors.

E-mail addresses: jaroslawserafin@ub.edu (J. Serafin), jumoreno@uniandes.edu.co (J.C. Moreno-Piraján).

<https://doi.org/10.1016/j.ces.2025.121222>

Received 6 July 2024; Received in revised form 24 December 2024; Accepted 14 January 2025

Available online 25 January 2025

0009-2509/© 2025 The Authors. Published by Elsevier Ltd. This is an open access article under the CC BY license (<http://creativecommons.org/licenses/by/4.0/>).

life, and significant chemical toxicity. It primarily exists as hexavalent uranium dissolved in the environment, displaying high solubility that allows easy movement through water sources, causing ecological and health risks.

This makes the efficient enrichment and separation of uranium from water sources crucial. Processes with strong adsorption capacity and selectivity have immense implications for public health, environmental protection, and sustainable nuclear energy. Several methods have been explored in the specialized literature for effective uranium separation, including adsorption, membrane filtration, chemical precipitation, electrocoagulation, and biological treatment (Torkabad et al., 2017; Zhao et al., 2011; Choi et al., 2020; Dubrawski et al., 2015; Li et al., 2017; Nariyan et al., 2018; Tapia-Rodriguez et al., 2010; Kumar et al., 2011; Gandhi et al., 2022; Zhang et al., 2022). However, each method has its limitations, ranging from high energy consumption in membrane filtration to economic feasibility in chemical precipitation.

Adsorption stands out as an economical and effective method for uranium enrichment and separation from radioactive wastewater, especially at low concentrations. Lignocellulosic biomass residues have gained prominence among various materials due to their customizable properties. Utilizing agricultural waste for adsorbent production and functionalization through biologic assembly presents a sustainable approach (Chen et al., 2018; Cheng et al., 2015; Ding et al., 2015; Huang et al., 2018; Zhu et al., 2018). These materials, derived from biomass, demonstrate enhanced uranium enrichment capabilities. Biomass sources range from natural biopolymers like cellulose, chitosan, and starch to biomass-carbon varieties such as activated carbon and hydrothermal carbon. Microbial materials like bacteria, fungi, and algae also find utility. Agricultural residues from crops, orchards, livestock, and forestry contribute to this approach (Li et al., 2023; Ma et al., 2012; Anirudhan et al., 2009; Bayramoğlu et al., 2006; Zänker et al., 2019; Jin et al., 2018; Hu et al., 2016; Sha et al., 2019; Chardi et al., 2022; Yelatontsev, 2023). Employing biomass-derived materials, particularly from agricultural residues, offers several advantages. Preparation methods can introduce diverse functional groups, enhancing material versatility and facilitating chemical interactions with uranyl ions. This ultimately improves adsorption capacity and selectivity toward uranyl ions. Secondly, the inherent renewable nature of biomass materials cannot be overlooked. Originating from sustainable sources like plant fibers and agricultural waste, these materials stand as an environmentally friendly choice, aligning with the principles of ecological responsibility.

This study has comprehensively explored the chemical and thermodynamic aspects of uranium adsorption using activated carbons derived from corn cob residues (Zea Mays). This research introduces pioneering insights that significantly advance our comprehension and broaden the horizons for the practicality of these materials in uranium adsorption. This work showcases advancements in uncovering the potential utility of activated carbons sourced from corn cob residues under various conditions. It examines their efficacy as adsorbents for uranium and investigates the feasibility of generating a viable scenario wherein these materials could potentially serve as suitable candidates. Through uranium enrichment and separation methodologies, these materials could find extended applications beyond uranium and be utilized for other radioactive substances. This research thereby offers a novel perspective on the potentially transformative role of activated carbons from corn cob residues.

The ever-increasing global energy demand, fueled by rapid economic growth, industrialization, and technological advancements, has driven the urgent need for alternative energy sources that prioritize safety, efficiency, environmental sustainability, and minimal carbon emissions. Traditional fossil fuels, such as oil, natural gas, and coal, have been extensively consumed, resulting in detrimental environmental impacts, including greenhouse gas emissions and global warming. As the world shifts towards cleaner energy solutions, nuclear energy has emerged as a pivotal alternative due to its ability to produce vast amounts of

electricity while maintaining a significantly lower carbon footprint compared to fossil fuels (Bharadwaj et al., 2023).

While nuclear energy holds great promise, its adoption has been met with debates, particularly regarding the risks associated with radioactive waste management. However, with careful application, rigorous safety protocols, and proper disposal methods, nuclear energy can play a vital role in addressing both energy security and environmental challenges. The use of nuclear energy offers a strategic pathway to reducing dependence on fossil fuels and mitigating the ecological impacts of climate change (Basak et al., 2023). Nonetheless, the advancement of nuclear energy brings heightened nuclear safety concerns, particularly in managing radioactive byproducts. Historical nuclear accidents have highlighted the importance of stringent controls, especially in preventing the release of harmful radionuclides during various human activities, including the disposal of spent nuclear fuel, uranium mineral processing, nuclear weapons production, and the use of radioactive materials in medical, industrial, and research applications (Burns et al., 2012; Huang et al., 2018; Spirin et al., 2015; Schulte-Herbrüggen et al., 2016).

In nations with operational nuclear power plants, the secure disposal of radioactive waste is a pressing global challenge, as radioactive materials pose significant long-term risks to ecosystems and human health. Among the most hazardous radioactive byproducts is uranium, a highly abundant element characterized by its potent radioactivity, chemical toxicity, and long half-life. Uranium primarily exists in its hexavalent form (U(VI)) in environmental systems, where its high solubility allows it to easily migrate through water sources. This mobility increases the risk of widespread contamination of groundwater and surface waters, thereby posing ecological and health risks to both aquatic ecosystems and populations relying on these water sources for drinking and agriculture (Burns et al., 2012; Huang et al., 2018; Spirin et al., 2015; Schulte-Herbrüggen et al., 2016). Efficient separation and recovery of uranium from water sources is thus critical to safeguarding public health and protecting the environment. Several technologies have been developed for the removal of uranium, including adsorption, membrane filtration, chemical precipitation, electrocoagulation, and biological treatment (Schulte-Herbrüggen et al., 2016; Torkabad et al., 2017; Zhao et al., 2011; Choi et al., 2020; Dubrawski et al., 2015; Li et al., 2017; Nariyan et al., 2018; Tapia-Rodriguez et al., 2010; Kumar et al., 2011; Gandhi et al., 2022; Zhang et al., 2022). However, each method presents certain limitations. For example, membrane filtration often involves high energy consumption, while chemical precipitation may have limited economic feasibility due to the production of secondary waste (Bharadwaj et al., 2023). Among these techniques, adsorption stands out as an economical, efficient, and scalable method for uranium enrichment and separation from radioactive wastewater, particularly at low uranium concentrations. Lignocellulosic biomass has gained prominence as an ideal precursor material for the development of adsorbents due to its renewable nature, wide availability, and highly customizable properties.

Agricultural residues, which are often underutilized, present an environmentally sustainable option for adsorbent production. The valorization of such residues into activated carbons, hydrothermal carbons, and biochars is an innovative approach for enhancing uranium adsorption (Kim et al., 2023). These biomass-derived materials, rich in functional groups such as hydroxyl, carboxyl, and phenolic groups, facilitate strong chemical interactions with uranyl ions (UO_2^{2+}), improving the adsorption capacity and selectivity of these materials toward uranium (Rajendran et al., 2024). Biomass sources, ranging from natural biopolymers like cellulose, chitosan, and starch to microbial materials like bacteria, fungi, and algae, have demonstrated enhanced uranium removal capabilities in previous studies (Li et al., 2023; Ma et al., 2012; Anirudhan et al., 2009; Bayramoğlu et al., 2006; Zänker et al., 2019; Jin et al., 2018; Hu et al., 2016; Sha et al., 2019; Chardi et al., 2022; Yelatontsev, 2023). Employing biomass-derived adsorbents, particularly from agricultural residues like corn cobs, offers several

advantages. The preparation of activated carbons through processes such as chemical activation (e.g., KOH treatment) and surface functionalization introduces diverse functional groups that enhance the versatility of the material and increase its affinity for uranyl ions. This, in turn, enhances the overall adsorption capacity and selectivity of the material, making it highly effective for uranium removal (Bharadwaj et al., 2023; Basak et al., 2023). Additionally, the inherent renewability and sustainability of biomass materials cannot be overlooked. Agricultural residues such as corn cobs are sourced from environmentally responsible practices and align with the principles of green chemistry and ecological responsibility (Basak et al., 2023).

Nitrogen-doped activated carbons synthesized from corn cob biomass offer a compelling alternative to other uranium sorbents such as MOFs, COFs, mineral sorbents, and synthetic resins due to their superior combination of performance, cost-effectiveness, and sustainability. While MOFs (metal-organic frameworks) and COFs (covalent organic frameworks) provide high adsorption capacities and customizable structures, their production is often hindered by high costs and energy-intensive synthesis involving expensive organic linkers and metals (Ge et al., 2024). These factors limit their scalability for large-scale uranium remediation applications. In contrast, nitrogen-doped activated carbons are derived from renewable and low-cost biomass, utilizing simple and scalable chemical activation processes that make them far more economical without sacrificing competitive adsorption performance (Li et al., 2016). Mineral sorbents, such as clays and zeolites, are inexpensive and abundant, but they typically exhibit lower adsorption capacities (20–30 mg/g) and slower kinetics compared to nitrogen-doped activated carbons, which can achieve capacities up to 51.66 mg/g and reach equilibrium within minutes. Additionally, the hierarchical pore structure and nitrogen functionalization in activated carbons provide superior selectivity for uranium, even in the presence of competing ions, a property often absent in mineral-based sorbents (Gan et al., 2023). Synthetic resins, while selective, are costly to produce, degrade over time, and are less environmentally sustainable. Activated carbons, by contrast, are robust, reusable, and derived from agricultural waste, aligning with green chemistry principles and the circular economy. Their production not only reduces environmental waste but also minimizes the ecological footprint associated with adsorbent manufacturing. Overall, nitrogen-doped activated carbons excel by offering a high-performance, low-cost, and sustainable solution for uranium adsorption. They combine the advantages of tailored porosity, rapid adsorption kinetics, and renewable feedstocks, making them a practical and environmentally responsible choice compared to MOFs, COFs, mineral sorbents, and synthetic resins. Their cost-to-performance ratio and scalability position them as an ideal material for large-scale uranium remediation efforts.

In this study, we comprehensively explore the chemical and thermodynamic aspects of uranium adsorption using activated carbons derived from corn cob residues (Zea Mays). The novelty of this research lies in the dual-functionalization approach, combining KOH chemical activation with nitrogen doping via urea impregnation to produce highly porous and functionalized adsorbents. This method significantly enhances the adsorption efficiency and selectivity of the material for uranium ions by increasing surface area and introducing nitrogen-containing functional groups (e.g., amines, amides, and pyridinic nitrogen), which improve the interaction between the adsorbent and uranyl ions (Rajendran et al., 2024). This work demonstrates the utility of nitrogen-doped activated carbons from corn cob residues under varying conditions, examining their efficacy as adsorbents for uranium enrichment and separation. Furthermore, the study investigates the broader feasibility of employing these materials for other radioactive substances, thus offering a transformative approach to managing nuclear waste.

2. Materials and methods

2.1. Materials

The corn cob was gathered from a bustling marketplace of Bogotá, Colombia. Before proceeding with the experiment, a comprehensive analysis was conducted to ascertain their fundamental composition, which revealed the following percentages by weight: cellulose (35.45 %), hemicellulose (36.75 %), lignin (16.45 %), humidity (8.76 %), and ash (5.59 %). The corn cobs were meticulously ground into a fine texture for the experiment and then sifted through a 40-mesh sieve to ensure uniformity.

2.2. Preparation of the activated carbons based on corn cobs

The preparation of activated carbon from corn cob residues (CC) involved several carefully optimized steps aimed at enhancing the material's adsorption capacity for uranium (VI) ions. First, the corn cob residues were washed thoroughly with household water, followed by exhaustive rinsing with deionized water to ensure the removal of any impurities or foreign residues that could affect the activation process. After washing, the residues were dried in an oven at 80 °C to remove moisture and then crushed to a 45-mesh size. This particle size was selected based on preliminary tests, optimizing surface area and material handling for activation. The chemical activation of the corn cob residues was performed using KOH as an activating agent in a single-step activation process.

CC and KOH were weighed separately in a 1:0.3 wt ratio (CC), which was chosen after optimization trials. This ratio ensures sufficient chemical activation, enhancing pore formation without overactivation, which could lead to the collapse of the carbon structure. The mixture was then placed in a perforated quartz boat, which allowed for uniform heat distribution and carbonization during activation. Before heating, nitrogen gas (N₂) was flowed over the sample for 1 h to purge the system of oxygen, preventing oxidation. This step is crucial to maintaining a controlled, inert atmosphere during activation, ensuring that the carbonization process occurs uniformly across the material.

The activation process itself was optimized for both temperature and heating rate. The furnace temperature was raised at a controlled rate of 5 °C per minute until reaching the target activation temperature of 700 °C. This temperature was selected after extensive optimization, where lower temperatures resulted in insufficient pore development and higher temperatures caused structural degradation. The temperature was maintained at 700 °C for 2 h, a duration chosen to ensure complete activation and sufficient time for micropore formation. These parameters were key to producing an activated carbon with high surface area and well-developed porosity, both critical for improving uranium adsorption. Once the activation period was complete, the furnace was allowed to cool naturally to 120 °C, and then the nitrogen flow was stopped. The activated carbon, labeled CCAK7, was removed from the furnace, ground to a 60-mesh size to increase the available surface area, and extensively washed with very dilute hydrochloric acid (HCl) and deionized water. This washing process was essential for removing residual KOH and other soluble impurities. The material was washed until the pH of the rinse water remained constant, ensuring chemical stability. Finally, the activated carbon was dried in a vacuum oven at 85 °C for 48 h to eliminate any remaining moisture. For the nitrogen-doped activated carbon (labeled CCAKN7), a similar process was followed, with the addition of urea to introduce nitrogen-containing functional groups. Corn cob, KOH, and urea were mixed in a 1:0.3:0.3 wt ratio (CC:KOH), and the same activation procedure was applied. The urea served as a nitrogen source, and during the thermal activation, it decomposed, incorporating nitrogen into the carbon matrix. This step introduced nitrogen functionalities (such as amine and pyridinic nitrogen groups), which are known to enhance adsorption by providing additional active sites for uranium ions. The optimization of the urea concentration was

critical to ensure that the nitrogen doping improved surface functionality without compromising the structural integrity of the carbon.

2.3. Characterization and batch adsorption study of porous Corncob-Derived adsorbents for Uranium removal

The characterization of the corn-cob-derived adsorbents involved a comprehensive analysis of their properties. Proximate analysis was performed using a TGA-2000 analyzer (Las Navas, Spain), while ultimate analysis was conducted with a CHNS/O elementary analyzer (Vario Micro Cube, Germany). Thermogravimetric assessments utilized a NETZSCH thermobalance (model: STA 449 F3 Jupiter), employing nitrogen as the carrier gas at 100 mL min⁻¹, with alumina crucibles and a heating rate of 20 K/min. N₂ adsorption-desorption isotherms were measured using an IQ2 instrument (Anton Paar QuantaTec Inc., Boynton Beach, U.S.) at 77 K. BET surface area (S_{BET}), total pore volume (V_{total}), and micropore volume (V_{micro}) were determined. Pore size distribution curves were generated using the Density Functional Theory (DFT) approach, alongside non-local density functional theory (NLDFT) and quenched Solid density functional theory (QSDFT) methods (Neimark et al., 2009; Rodríguez-Reinoso et al., 1989; Rouquerol et al., 2007; Brunauer et al., 1938; Ravikovitch and Neimark, 2006; Olivier, 1998; Stoeckli et al., 2002; Py et al., 2003; Carrott and Carrott, 1999; Michot and Villieras, 2006; Seifi et al., 2016; Tascón, 2012).

Surface chemistry was investigated through Fourier transform infrared (FTIR) spectroscopy, using KBr pellets and a Nicolet 6700 FTIR spectrometer. Morphological examination utilized a scanning electron microscope (SEM, model: 6490-LV) at 10 kV, with samples coated in gold for enhanced conductivity.

The batch adsorption study explored the efficiency of corn-cob-derived porous adsorbents in removing U(VI) from aqueous solutions. Experiments were carried out in 100 mL PET bottles within a Thermo Scientific Tube Revolver operating at 70 rpm. Each bottle contained 15 mg of sample and 50 mL of U(VI) solution with varying concentrations (1.0 to 100.0 ppm). pH adjustments were made using HCl and NaOH solutions. After agitation, supernatant concentrations were determined using inductively coupled plasma optical emission spectrophotometry (ICP-OES, Perkin Elmer Optima 2000 DV). All data represent mean values from three separate runs. Negative controls using UO₂²⁺ solution without sorbent material were included.

The uranium adsorption q_e (mg U·g⁻¹ dry adsorbent) was calculated using the following formula:

$$q_e = \frac{(C_o - C_e)V}{W} \quad (1)$$

Where: q_e stands for the adsorption capacity of the adsorbent (mg·g⁻¹), C_o denotes the initial concentration of U(VI) (mg·L⁻¹), C_e signifies the equilibrium concentration of U(VI) (mg·L⁻¹), V represents the volume of the testing solution, and W indicates the weight of the adsorbent.

2.4. Uranium adsorption on activated carbons: equilibrium, kinetic and thermodynamic study

The aim of this study was to comprehensively examine the interaction between adsorbate (uranium) and adsorbent (activated carbon). Initial tests, though not included in this work, revealed pH 6.0 as optimal for maximum uranium adsorption capacity. Consequently, all tests were conducted under this pH value. Equilibrium behavior, kinetics, and thermodynamics of uranium adsorption were investigated. Equilibrium studies were performed across various temperatures (298 K, 308 K, 318 K, and 328 K), each involving uranium concentration (U(VI)) set at 100 ppm. Adsorption isotherms were constructed accordingly. The batch method was employed to analyze the U(VI) ion adsorption capacity of the activated carbons. In this procedure, uranium solutions were combined with respective activated carbons in Erlenmeyer flasks, stirred

using a magnetic stir bar, and maintained at designated temperatures for specific time intervals. Subsequently, 5 mL aliquots were withdrawn and processed through a syringe filter (0.65 µm membrane filter) to separate activated carbons. The concentration of U(VI) in the resultant solutions was quantified using an inductively coupled plasma-optical emission spectrophotometer (ICP-OES), specifically the Perkin Elmer Optima 2000 DV instrument. The sorption capacity (q_t) of U(VI) (mg·g⁻¹) was calculated using the following equation:

$$q_t = \frac{(C_o - C_t)V}{W} \quad (2)$$

To analyze the results obtained in the equilibrium studies, they were fitted to the Langmuir model, the Freundlich model, the Elovich model, and the intraparticle diffusion model. Kinetic studies were performed by varying U(VI) concentrations: 20, 40, 60, 80, and 100 mg L⁻¹ at 298 K temperature. The experimental results were fitted to the pseudo-first order, pseudo-second order, Elovich, and intraparticle models to analyze the kinetic behavior of U(VI) adsorption on the materials prepared from corn gopher. The kinetic and equilibrium models' parameters were estimated through non-linear regression using the software Origin 2018. The quality of the fit was statistically evaluated using the correlation coefficient (R²). Finally, the thermodynamic behavior of the uranium-activated carbon interactions was investigated. The thermodynamic variables were evaluated as follows: Gibbs free energy (ΔG°), change in enthalpy (ΔH°), and change in entropy (ΔS°). For the determination of these parameters, the results of the experiments with equilibrium adsorption curves at different temperatures (298 K, 308 K, 318 K, and 333 K) for the same initial uranium concentrations have been used. Again, the solutions were adjusted to the optimum pH. Contact was maintained for 360 min.

To assess the findings from the equilibrium studies, the data was fitted to various models including the Langmuir, Freundlich, Elovich, and intraparticle diffusion models. The investigation of kinetics involved altering U(VI) concentrations (20, 40, 60, 80, and 100 mg L⁻¹) at a temperature of 298 K. To examine the kinetic characteristics of U(VI) adsorption onto the corn gopher-derived materials, the experimental outcomes were matched with the pseudo-first order, pseudo-second order, Elovich, and intraparticle models. The estimation of model parameters was executed via non-linear regression using Origin 2018 software, while the fit's quality was statistically assessed using the correlation coefficient (R²). Subsequently, the thermodynamic traits of uranium-activated carbon interactions were explored. The thermodynamic attributes, including Gibbs free energy (ΔG°), alteration in enthalpy (ΔH°), and shift in entropy (ΔS°), were analyzed. These parameters were determined based on the outcomes of experiments encompassing equilibrium adsorption curves at different temperatures (298 K, 308 K, 318 K, and 333 K) while maintaining a consistent initial uranium concentration. Once more, the solutions were adjusted to the optimal pH level and allowed to interact for a duration of 360 min.

3. Results

3.1. Ultimate analysis

Table 1 presents the ultimate and proximate analyses for the raw corn cob (CC), KOH-activated sample (CCAK7), and urea-doped activated carbon (CCAKN7). The results illustrate significant changes in elemental composition and material properties as a result of chemical activation and nitrogen doping. See (Fig. 1).

A key observation is the substantial increase in the carbon content following activation. The carbon content of the raw corn cob (CC) was 59.53 %, which increased to 78.67 % in the KOH-activated sample (CCAK7) and further to 81.56 % in the nitrogen-doped sample (CCAKN7). This significant rise in carbon percentage reflects the effectiveness of the activation process, during which volatile compounds and oxygen-containing functional groups are removed, enriching the carbon

Table 1

Characterization of the maize gopher and the samples prepared from this material.

Ultimate analysis (% wt/wt)	CC	CCAK7	CCAKN7
Carbon	59.53	78.67	81.56
Hydrogen	7.76	8.95	9.56
Nitrogen	2.34	4.67	6.87
Oxygen	30.37	7.71	2.01
Elemental Analysis proximal (% wt/wt)			
Volatile matter	50.70	20.59	8.81
Fixed carbon	29.64	59.53	71.45
Ash	5.54	4.76	4.98
Moisture content	17.12	15.12	14.76

structure. The KOH activation not only facilitates carbonization but also enhances porosity by promoting the development of a microporous structure, as evidenced by the increase in fixed carbon from 29.64 % in the raw corn cob to 59.53 % in CCAK7 and 71.45 % in CCAKN7. These values indicate a more robust carbon framework in the activated samples, which directly correlates to higher adsorption capacities.

The decrease in oxygen content further highlights the chemical changes induced by activation. The oxygen content of the raw corn cob (CC) was 30.37 %, which dropped drastically to 7.71 % in CCAK7 and 2.01 % in CCAKN7. This reduction in oxygen is consistent with the removal of volatile matter and oxygenated functional groups during activation (López-Francés et al., 2024), contributing to the increased hydrophobicity and stability of the material. Such structural changes are essential for enhancing adsorption capacity, as a higher carbon content coupled with lower oxygen enables more effective interactions with adsorbates, such as uranium ions, in aqueous solutions.

Another notable change is observed in the volatile matter content, which decreased from 50.70 % in the raw material to 20.59 % in CCAK7 and further to 8.81 % in CCAKN7. The reduction in volatile matter signifies the removal of non-carbon elements during thermal treatment, leaving behind a purer, more concentrated carbon structure. The low volatile content in activated carbon CCAKN7 indicates a more stable material with enhanced thermal resistance, which is critical for long-term application in adsorption processes.

Ash content is a critical factor in the preparation of adsorbents, as excessive ash can block the pores and hinder adsorption performance. In

this study, the ash content of the raw corn cob (CC) was 5.54 %, which decreased slightly to 4.76 % in CCAK7 and 4.98 % in CCAKN7. The relatively low ash content in both activated samples suggests that the activation process was successful in removing inorganic residues, leaving behind a highly porous structure without significant blockage by ash. This ensures that the porosity created during activation is available for adsorption, which is essential for achieving high adsorption efficiencies.

The nitrogen content is particularly important in the context of the activated carbon CCAKN7. The nitrogen content in the raw corn cob (CC) was 2.34 %, which increased to 4.67 % in CCAK7 due to partial incorporation of nitrogen during the activation process. However, in CCAKN7, the nitrogen content increased dramatically to 6.87 %. This increase is attributed to the incorporation of nitrogen-containing functional groups such as amines and pyridinic nitrogen through urea doping during activation. These functional groups are known to enhance the chemical reactivity of the surface and provide additional binding sites for adsorbates, particularly for metal ions like uranium (Ma et al., 2024). The higher nitrogen content in CCAKN7 suggests improved interaction capabilities with uranium ions, making this sample more effective in adsorption applications.

Moisture content decreased slightly across the samples, from 17.12 % in the raw corn cob to 15.12 % in CCAK7 and 14.76 % in CCAKN7. The lower moisture content is desirable as it indicates better stability and hydrophobicity, which reduces the likelihood of water interference during adsorption.

Table 1 shows the results obtained for the last analysis corresponding to the corn cob (CC), the sample activated with KOH (CCAK7), and the sample activated with urea (CCAKN7). The results are very interesting when compared; for example, the difference between the ash content of maize cob and the samples prepared from this material is significant because the latter has a low ash content (2.54 % by weight).

The fact that the % ash is low allows the pores not to be blocked by the presence of this material during inert atmosphere processing. When the CC is activated and a new analysis is performed, both next and last, it is observed (as shown in Table 1) that the carbon% increases significantly and the ash% remains low. This shows that the prepared materials have a high carbon content and that the effect of treating with urea on the CCAKN7 sample was sufficient, presenting the highest % of N, as

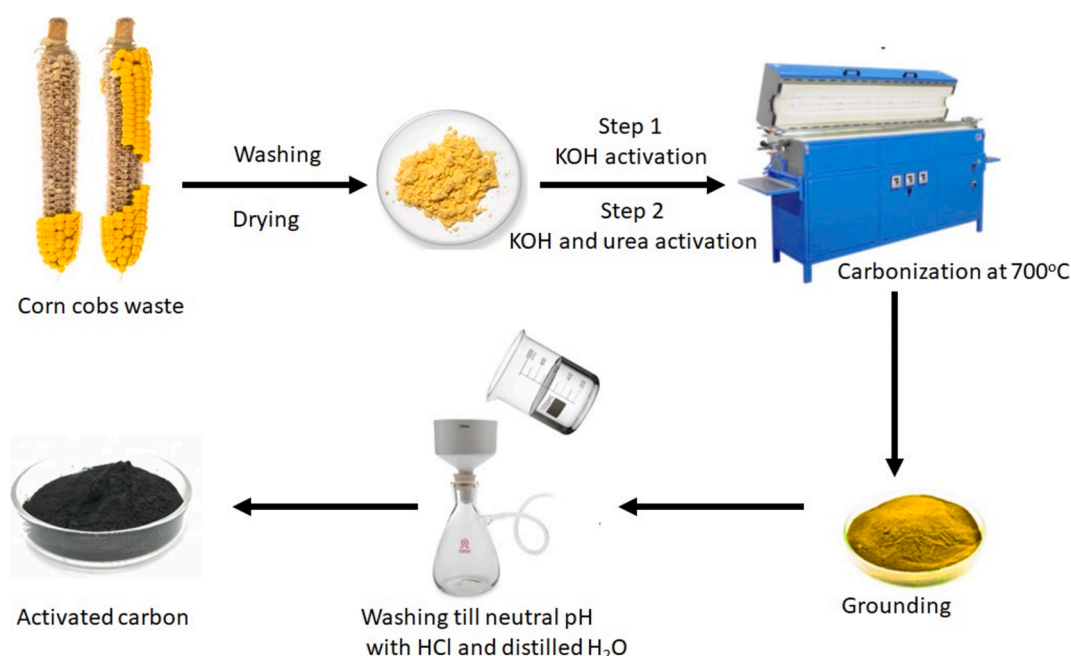


Fig. 1. Schematic preparation of activated carbons from corn cobs waste.

shown in Table 1.

3.2. Thermogravimetric analysis

Subject to thermogravimetric analysis in a non-reactive environment with nitrogen as the inert gas, the primary substance (CC) was heated at 10 °C per minute. The outcomes of this analysis are visually presented in Fig. 2. Within the graphical representation of Fig. 2, discrete stages in the thermogravimetric analysis (TGA) are evident:

1. Phase (I) involves a preliminary drying process that eliminates stored moisture and evaporates light components from the sample. This phase occurs at temperatures below 100 °C.
2. Phase (II) pertains to the degassing of biomass and is observed within the temperature range of 100–310 °C.
3. Phase (III) marks the decomposition of lignocellulosic compounds and commences at 310 °C, stabilizing around 550 °C.

Concerning the corncob sample under the specific experimental conditions applied, the TGA outcomes reveal the following insights:

- Phase I: The biomass dehydration occurs below 100 °C.
- Phase II: Notably, a substantial decomposition phase takes place, particularly marked by rapid devolatilization around 330–350 °C. This results in a considerable mass reduction of 73.7 %. This stage aligns with the decomposition of fundamental constituents such as hemicellulose, cellulose, and lignin. Notably, hemicellulose decomposes between 200–350 °C, cellulose between 350–500 °C, and some lignin also degrades within this range (Viet et al., 2015; Gani and Naruse, 2007; Sonobe et al., 2006).
- Phase III: In the temperature interval of 400–600 °C (Phase III), a relatively smaller mass reduction of 10.9 % is observed, compared to the maize cob sample. This decline is attributed to residual lignin. Furthermore, an exothermic polymerization stage of the char is observed, continuing some of the cellulose-lignin crosslinking (López-Francés et al., 2024; Ma et al., 2024; Viet et al., 2015). It's worth mentioning that the TGA outcomes for the CCAK7 and CCAKN7 samples exhibit slight deviations compared to the initial material (CC), showing slightly diminished weight loss.

The TGA of the corn cob (CC), KOH-activated (CCA7), and nitrogen-doped (CCA7N) samples provides a detailed understanding of the thermal degradation behavior and stability of these materials under

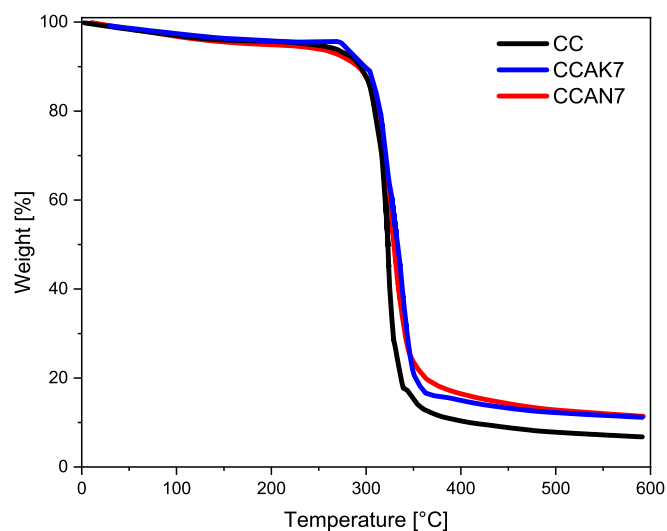


Fig. 2. TGA thermograms of samples of activated carbons: CC (black); CCAK7 (blue); CCA7N (red).

a controlled heating regime in a nitrogen atmosphere. The TGA results, obtained by heating the samples at a rate of 10 °C per minute, reveal key stages of thermal decomposition that reflect the breakdown of biomass components and the transformation of these materials into activated carbons.

In the case of the raw corn cob (CC), the initial phase of decomposition occurs below 100 °C, where moisture and light volatiles are evaporated, resulting in minor mass loss. This phase is essential for removing free water from the biomass, preparing it for the subsequent thermal degradation of its organic components. As the temperature increases, the second phase of decomposition occurs between 100 °C and 310 °C, where significant mass loss is observed. Approximately 73.7 % of the initial mass is lost during this phase due to the thermal breakdown of hemicellulose, cellulose, and some lignin, which are the primary structural components of lignocellulosic biomass (Shapiro et al., 2023). Hemicellulose typically decomposes between 200 °C and 350 °C, while cellulose undergoes pyrolysis between 350 °C and 500 °C. This stage is marked by the release of volatile gases and other byproducts, reflecting the high volatile content of the raw biomass (Hernowo et al., 2024). The thermal degradation of these polymers leads to the formation of a char structure that becomes the basis for carbon formation in later stages.

As the temperature reaches 400 °C, the third phase of decomposition begins, extending to 600 °C. This phase is characterized by the slower breakdown of residual lignin, which decomposes over a broader temperature range due to its higher thermal stability compared to hemicellulose and cellulose. The mass loss during this phase is approximately 10.9 %, and the process is accompanied by the onset of carbonization, where exothermic polymerization and crosslinking reactions stabilize the carbon matrix (Ghahri and Park, 2023). The formation of char during this phase is crucial for creating a carbon-rich structure, which is essential for producing activated carbon with good adsorption properties.

In contrast, the TGA curves for the activated samples, CCAK7 and CCAKN7, demonstrate improved thermal stability compared to the raw corn cob. The chemical activation process using KOH significantly alters the thermal decomposition behavior of the biomass. In CCAK7, the activation process removes a substantial portion of the volatile components during preparation, resulting in a more carbon-rich and thermally resistant structure. This is evidenced by the reduced mass loss in the second phase of decomposition compared to CC, indicating that much of the hemicellulose and cellulose content has already been removed during the activation process. The lower mass loss in the third phase further suggests that KOH activation enhances the development of a stable, carbonaceous structure with a higher fixed carbon content and fewer thermally unstable components (Zhang et al., 2023). This improvement in thermal stability is critical for enhancing the adsorption capacity of the activated carbon, as a more stable material can withstand repeated adsorption-desorption cycles and perform better under challenging environmental conditions.

Similarly, the nitrogen-doped sample, CCAKN7, exhibits enhanced thermal stability compared to CC and even CCAK7. The incorporation of nitrogen through urea doping introduces functional groups that contribute to the stabilization of the carbon matrix during activation (He et al., 2024). Nitrogen-containing groups, such as pyridinic and pyrrolic nitrogen, promote crosslinking within the carbon structure, increasing its thermal resistance. The reduced mass loss in both the second and third phases for CCAKN7 indicates that the nitrogen doping process not only enhances the material's stability but also leads to the formation of a more robust and carbonized structure. This increased stability is advantageous for adsorption applications, as nitrogen doping introduces additional active sites for binding target contaminants, such as uranium ions, while also improving the material's overall resilience.

When comparing the three samples, it is evident that both KOH activation and nitrogen doping significantly improve the thermal properties of the materials. The raw corn cob undergoes substantial mass loss due to the decomposition of volatile organic components, whereas

the activated samples, CCAK7 and CCAKN7, exhibit reduced weight loss and enhanced thermal stability. KOH activation leads to a more carbonized structure with a higher fixed carbon content, while nitrogen doping further stabilizes the material by introducing nitrogen-containing functional groups that enhance crosslinking and thermal resistance (Barker-Rothschild et al., 2025). These modifications result in activated carbons that are more suitable for adsorption applications, with improved thermal stability, higher carbon content, and enhanced reactivity, particularly for the removal of uranium ions from aqueous solutions.

3.3. Fourier transformation infrared spectra (FT-IR)

The FT-IR absorption spectra of the corn cob agricultural residue (CC) and the activated carbons derived from it (CCA7 and CCAKN7) are presented in Fig. 3.

In the spectrum of CC, notable peaks are observed that correspond to the major functional groups present in lignocellulosic materials. The broad absorption near 3330 cm^{-1} reflects the presence of O-H groups, possibly linked to the symmetric arrangement of methyl and methylene groups within hemicellulose, cellulose, and lignin. Furthermore, there are peaks in the fingerprint region between 1000 cm^{-1} and 1500 cm^{-1} , which can be attributed to C-O and C-H bending vibrations (Kumar et al., 2024). A peak at 1375 cm^{-1} is associated with C-H bending rather than C=O stretching, which reflects the presence of methyl groups in the sample. The peak at 1630 cm^{-1} aligns with the C=C stretching vibration, indicative of aromatic content within lignin. Additionally, the peak at 2980 cm^{-1} corresponds to C-H stretching vibrations, which are typically associated with aliphatic hydrocarbons present in lignocellulosic materials (Kumar et al., 2024).

Activated carbon CCAK7 reveals several modifications that occur during the activation process. The broad spectral bands between 3450 cm^{-1} and 2360 cm^{-1} correspond to O-H stretching vibrations and symmetric C-H stretching from CH_2 groups, suggesting a more complex surface structure following activation. The most prominent peak in the spectrum is located at 1700 cm^{-1} , which corresponds to C=O stretching vibrations. This peak is characteristic of carbonyl groups, indicating the introduction or exposure of carboxylic acids, esters, or other oxygenated groups during the activation process. The vibrational band at 1060 cm^{-1} is attributed to C-O-C stretching vibrations, likely from ether groups or glycosidic bonds in the remaining polysaccharide structures (Gieroba et al., 2023). The vibrational band at 1650 cm^{-1} is associated with C=C

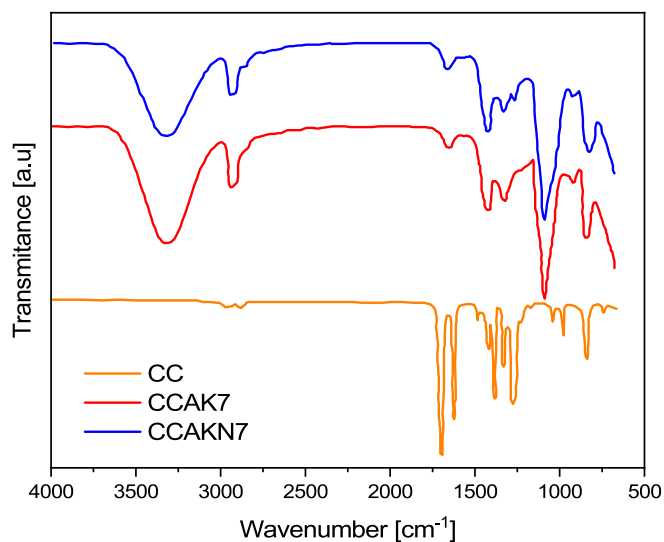


Fig. 3. FTIR spectra for activated carbons: a) CC (red); b) CCAK7 (blue); c) CCAKN7 (black).

stretching vibrations within the aromatic rings, which likely originate from lignin content that remains after activation. Additionally, the peak at 1008 cm^{-1} corresponds to C-H bending vibrations, associated with aromatic and phenolic structures that are typically seen in activated carbons derived from lignocellulosic biomass.

The spectrum of activated carbon CCAKN7 reveals further chemical modifications due to urea impregnation. Notable peaks at 2940 cm^{-1} , 1670 cm^{-1} , and 1510 cm^{-1} correspond to C-H stretching, C=O stretching, and C-N stretching vibrations, respectively. The appearance of the peak at 1570 cm^{-1} , which is absent in both CC and CCAK7, is attributed to C-N stretching vibrations, a clear indicator of nitrogen functionalization introduced through urea impregnation. This feature distinguishes CCAKN7 from the other two samples, reflecting the successful incorporation of nitrogen into the activated carbon structure. Additional peaks at 2940 cm^{-1} and 1380 cm^{-1} are associated with C-H stretching in CH_2 groups and asymmetric stretching of C-O-C bonds, respectively, suggesting the presence of ether linkages or other oxygen-containing functionalities in the sample. Moreover, absorption peaks at 970 cm^{-1} and 860 cm^{-1} are linked to out-of-plane bending vibrations of CH_2 and C-O stretching, respectively, further supporting the structural modifications introduced during the activation process and nitrogen doping.

3.4. Scanning electron microscopy (SEM)

The SEM micrographs presented in Fig. 4 offer valuable insights into the morphological changes of the raw corn cob (CC) and the activated carbon samples (CCA7 and CCAKN7) produced in this study. These images reveal the structural transformation of the materials during the chemical activation and urea-doping processes, illustrating the development of porosity, which is critical for enhancing the adsorption properties of activated carbons.

In Fig. 4a, the SEM image of the raw corn cob (CC) shows an intact, unmodified surface composed of thin, tubular structures characteristic of lignocellulosic biomass. The visible light, fibrous tubes are densely packed, with minimal porosity observed on the surface. These tubes represent the natural vascular bundles of the corn cob, responsible for water and nutrient transport in the plant. While this unmodified structure reflects the inherent features of agricultural residues, it is not yet optimized for adsorption applications due to the lack of sufficient pore volume and surface area.

Upon activation with KOH, as seen in Fig. 4b (CCA7), the SEM reveals significant structural modifications. The most notable change is the appearance of larger and more defined pores throughout the carbon matrix. This increased porosity is a direct result of the chemical activation process, during which KOH acts as a pore-forming agent. During pyrolysis, KOH facilitates the removal of volatile organic compounds and enhances the development of a microporous and mesoporous structure by etching away portions of the carbon framework. This leads to the creation of interconnected pores, which are critical for improving the material's surface area and accessibility to adsorbates. The pore enlargement seen in CCA7 is a crucial factor that enhances its adsorption capacity for contaminants, such as uranium ions, by providing more active sites and channels for diffusion. Furthermore, small accumulations observed in the SEM image correspond to residual potassium salts, a byproduct of the activation process. These residues are typically removed during the washing stage, which ensures the purity and functionality of the final activated carbon.

Fig. 4c illustrates the SEM micrograph of CCAKN7, the nitrogen-doped sample activated with both KOH and urea. This image shows a further enhancement in the pore size and number, with a more complex and highly porous surface compared to CCA7. The impregnation of the raw corn cob with urea prior to activation not only introduces nitrogen functional groups into the carbon matrix but also plays a role in promoting additional porosity. The urea decomposes during pyrolysis, releasing gases such as ammonia and carbon dioxide, which assist in

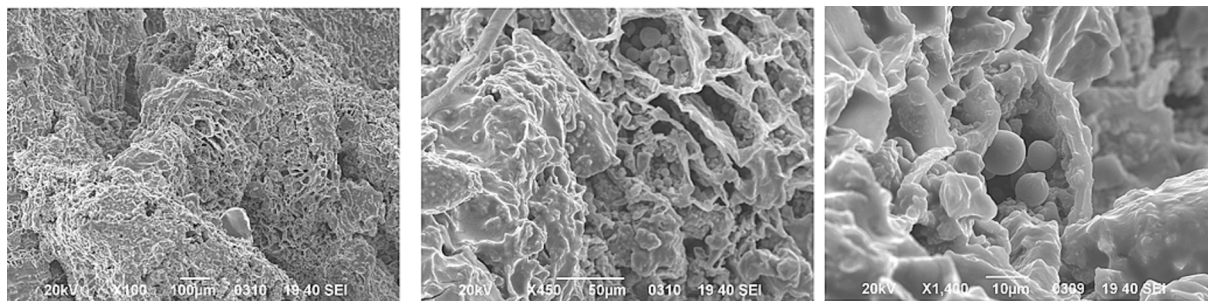


Fig. 4. SEM micrographs of a) raw corncob (CC); b) CCAK7; c) CCAKN7.

expanding the pore structure and increasing the overall surface area of the material. The presence of larger, well-defined pores in CCAKN7, compared to CCAK7, indicates that urea plays a significant role in further developing the pore architecture. This enhanced porosity is beneficial for adsorption applications, as it allows for more efficient diffusion of larger molecules, such as uranium ions, and increases the number of active sites available for chemical interactions. The nitrogen functionalities introduced through urea doping may also contribute to improving the adsorption affinity for metal ions by providing electron-donating sites that can form stronger bonds with adsorbates.

The morphological differences observed between the raw corn cob (CC), CCAK7, and CCAKN7 highlight the effectiveness of chemical activation and nitrogen doping in modifying the carbon structure to enhance porosity and surface area. In the case of CCAK7, the activation with KOH leads to a well-developed porous structure, but the addition of urea in CCAKN7 further optimizes this structure, producing a material with superior porosity and nitrogen functionality. These differences in porosity are further supported by the data in Table 2, which shows a significant increase in the BET surface area and pore volume of CCAK7 and CCAKN7 compared to the raw corn cob. The higher surface area and pore volume, particularly in CCAKN7, are consistent with the SEM observations of enhanced porosity. This structural transformation is critical for applications in environmental remediation, as a larger and more accessible pore structure allows for better adsorption performance. The enhanced porosity in CCAKN7, combined with the introduction of nitrogen groups, suggests that this material has great potential for use in the adsorption of heavy metals and other contaminants from aqueous solutions.

3.5. N_2 adsorption–desorption isotherms

Fig. 5 illustrates the adsorption–desorption isotherms obtained at 77 K for the three samples investigated in this study, namely CC, CCAK7, and CCAKN7. These isotherms are classified as type Ib according to the International Union of Pure and Applied Chemistry (IUPAC) classification system (Brunauer et al., 1938). This classification indicates that the materials possess a predominantly microporous architecture with pore sizes extending from larger micropores (diameters less than 2 nm) to more confined mesopores (diameters between 2 and 50 nm), consistent with the structural characteristics typically observed in porous carbons (Thommes et al., 2015; Li et al., 1998). The type Ib isotherm is marked by a steep rise in adsorption at low relative pressures ($P/P_0 < 0.1$), signifying the filling of micropores through micropore condensation, a

Table 2

Parameters of the porous structure of activated carbons produced from corncobs.

Sample	S_{BET} ($m^2 g^{-1}$)	r (nm)	$V_{total}(CC)$ (g^{-1})	$V_{micro}(CC)$ (g^{-1})	$V_{meso}(CC)$ (g^{-1})
CCAKN7	1395	0.95	0.65	0.55	0.10
CCA7	915	1.15	0.45	0.34	0.11
CC	563	0.86	0.38	0.25	0.13

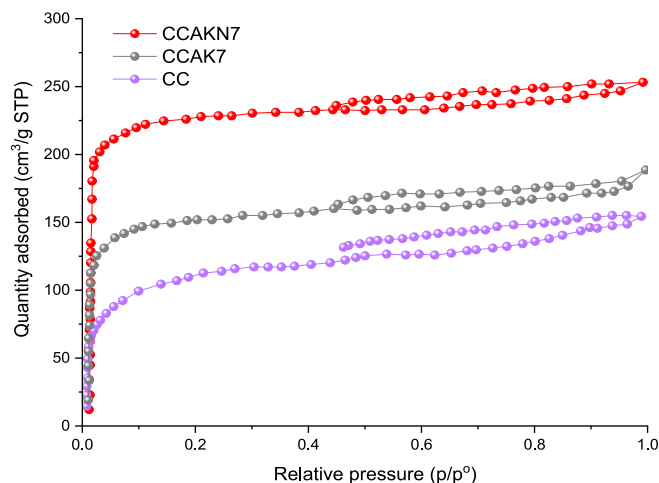


Fig. 5. The N_2 adsorption isotherms for CCAKN7, CCAK7, and CC samples.

process that occurs due to the high adsorption potential exerted in such narrow pores. Among the three samples, CCAKN7 exhibits the highest nitrogen adsorption capacity, followed by CCAK7 and then CC. This trend indicates that the structural modifications applied during the preparation of CCAK7 and CCAKN7 significantly enhanced their porosity compared to the unmodified CC sample. The differences in nitrogen adsorption volume suggest variations in micropore volume, surface area, and potentially the chemical properties of the pore surfaces, such as the introduction of heteroatoms or functional groups that enhance interactions with nitrogen molecules. See (Table 3).

The isotherms also display a pronounced hysteresis loop, a characteristic feature of materials containing mesopores. In this case, the hysteresis loop is observed within the relative pressure range of 0.45 to 0.9 (P/P_0), which corresponds to the capillary condensation and delayed desorption processes typical of mesoporous structures. The presence of a

Table 3

Thermodynamic parameters of U(VI) adsorption on activated carbon ($Co = 100$ ppm; time = 360 min; pH = 5.00).

Sample	T (K)	ΔG° ($kJ.mol^{-1}$)	ΔH° ($kJ.mol^{-1}$)	ΔS° ($J.(mol.K)^{-1}$)
CCAKN7	298	-32.45	-94.65	-158.32
	303	-37.75		
	308	-39.84		
	313	-41.66		
CCA7	298	-32.38	-65.34	-94.57
	303	-28.34		
	308	-26.32		
	313	-23.45		
CC	298	-30.21	-52.81	-77.34
	303	-28.12		
	308	-24.37		
	313	-21.32		

hysteresis loop reflects the interplay between adsorption and desorption mechanisms, where mesopores allow for capillary condensation at higher pressures, but their evacuation during desorption is delayed due to factors such as pore connectivity and geometry. The shape of the hysteresis loop aligns with the IUPAC-defined Type H4 classification, which is characteristic of materials with narrow slit-like pores (Roth et al., 2016). These slit-like pores are often associated with layered or lamellar structures and are indicative of a pore network that combines microporosity with a fraction of narrow mesopores. The desorption branch, which deviates significantly from the adsorption branch, highlights the restricted pore openings or “necks” in the mesoporous regions, which hinder the desorption process and contribute to the observed hysteresis behavior.

The combined analysis of the type Ib isotherms and Type H4 hysteresis loops suggests that the primary structure of the materials is microporous, but with secondary contributions from mesopores that enhance their overall textural properties (Donohue and Aranovich, 1998). The microporous framework dominates the adsorption behavior at low relative pressures, providing a high surface area and strong adsorption potential, while the presence of mesopores improves molecular diffusion and accessibility, making the materials versatile for a range of adsorption applications. The hierarchical pore structure inferred from these features is particularly advantageous, as it offers a balance between adsorption efficiency and transport properties. Notably, the superior nitrogen adsorption capacity of CCAKN7 compared to CCAK7 and CC implies a higher density of active sites and an optimized pore structure, likely resulting from its tailored activation and functionalization processes. These modifications not only increase the micropore volume but also introduce mesopores or enhance pore interconnectivity, thereby improving the material’s ability to adsorb and retain nitrogen molecules.

Interestingly, a comprehensive exploration of adsorption isotherms, delineating relative pressures on a semilogarithmic scale (Fig. 6), opens the door to a more intricate analysis compared to the insights garnered from the conventional N₂ adsorption isotherms at 77 K on a linear scale (Park and Jung, 2003). This graphical representation can be effortlessly constructed using the same software employed for the sortometer in this study or through an Excel spreadsheet. These plots facilitate a profound examination of the diffusion mechanisms of nitrogen molecules within the intricate porous framework of each sample. Moreover, they unveil potential distinctions in the structural attributes of the studied materials, particularly in the realm of low P/P⁰ pressures (Ryu et al., 2000; Yakout and El-Deen, 2016). The exploration of nitrogen adsorption onto the prepared porous solids in this investigation can be classified into distinct

stages, as noted by other researchers (Stoekli et al., 2002). This classification, visualized through semilogarithmic graphs, unfolds in five distinct phases:

a) 10⁻⁶ – 10⁻⁴, b) 10⁻⁴ – 10⁻², c) 10⁻² – 10⁻¹, d) 0.1–0.9, and e) 0.9–1.0.

These stages, as substantiated by the existing scientific literature (Gani and Naruse, 2007; Sonobe et al., 2006; Shapiro et al., 2023; Hernowo et al., 2024; Ghahri and Park, 2023), correspond to intricate multi-stage filling processes (Ghahri and Park, 2023; Zhang et al., 2023), specifically:

(i) The ingress of nitrogen into narrow micropores. (ii) Formation of a monolayer on the surfaces of broader micropores, including supermicropores. (iii) Penetration into these broader micropores. (iv) Monolayer creation and mesopore filling via capillary condensation. (v) Macropore infiltration through capillary condensation predominantly transpires at relative pressures approaching unity. In summary, it can be said that, by using this type of graphical representation, it is possible to make an adequate interpretation of the entry of N₂ molecules into the porous system with the results obtained by nitrogen sorptometry for the prepared samples. In the 10⁻⁶-10⁻⁴ zone, the CC and CCAK7 samples show a slight increase in the entry of nitrogen molecules, which is associated with filling the micropores. In contrast, the CCAKN7 sample shows a more pronounced increase, corresponding to the filling of the narrow micropores. In the 10⁻⁴-10⁻² zone, it is observed that the CC sample shows a slight and constant increase as the nitrogen molecules enter its pores, whereas, in the CCAK7 and CCAKN7 samples, there is a strong change during the adsorption of nitrogen molecules. This is associated with wider micropores, such as supermicropores. In the 10⁻²-10⁻¹ zone, the three samples show a continuous increase during N₂ adsorption. This is associated with the end of monolayer formation and the beginning of condensation. Finally, in the 0.9–1.0 zone, the three samples show the same behavior. The filling corresponds to that of the macropores. In addition, Fig. 6 shows that both CC, CCAK7, and CCAKN7 have significant nitrogen adsorption in the range of relative pressures between 10⁻³-10⁻¹. This allows us to conclude that all the samples prepared in this work have a large part of their pores, such as supermicropores and wider micropores.

Table 2 shows the textural properties of the materials prepared in this work. BET surface area, micropore, mesopore, and total pore volumes are given. Total pore volume, V_{total}, was calculated from nitrogen adsorption data at 77 K as the volume of liquid nitrogen at 0.95 relative pressure. The micropore volume, V_{micro}, was determined by the D.R. method. The mesopore volume, V_{meso}, was obtained by subtracting the micropore volume from the total pore volume. It can be observed that the samples show a good evolution of the BET surface area, which is between 1395 and 563 m².g⁻¹. While the total pore volume, the CCAKN7 > CCAK7 > CC. In general, the increase in porosity can be attributed to the release of tars due to the combination of the effect of temperature and the effect of the respective activating agent. From the results, it can be concluded that these tars come out under the experimental conditions used, and they don’t block the pores.

The pore size distribution (PSD) of ACs is shown in Fig. 7. These DFT pore size distributions are shown for activated carbons prepared from corn gopher. The PSD plot shown in Fig. 7 (only the lower part of the porosity is shown) shows a hierarchical pore structure with a maximum of around 0.4 nm for all the samples. This indicates that the activation process was effective for both starting material (corn gopher), KOH, and urea, producing samples with basic micropore development. It should be noted, however, that a certain amount of mesoporosity was generated. The intensity of these peaks, around 0.4 nm, is directly related to the activation conditions and the impregnating agent used to obtain the respective activated carbon. It can be seen that compared to the CC and CCAK7 samples, the activated carbon produced with urea shows the strongest peak with a pore width of 0.4 nm. They show that the samples developed mesoporosity in the graph (not shown here) for the PSD at larger pore widths.

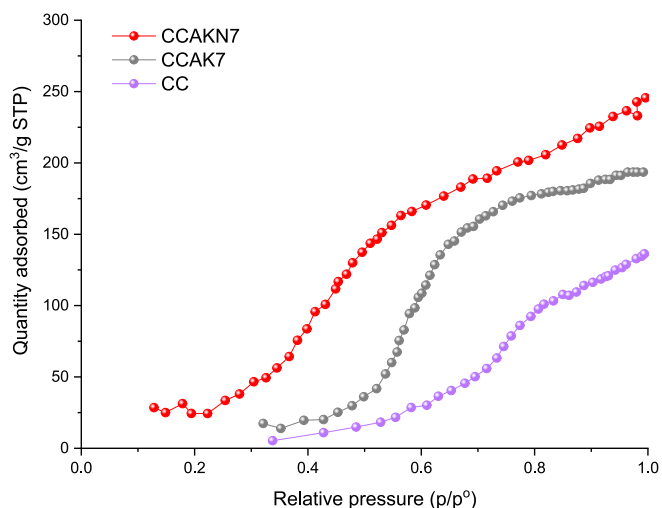


Fig. 6. The adsorption isotherms across relative pressures exhibited on a semilogarithmic scale.

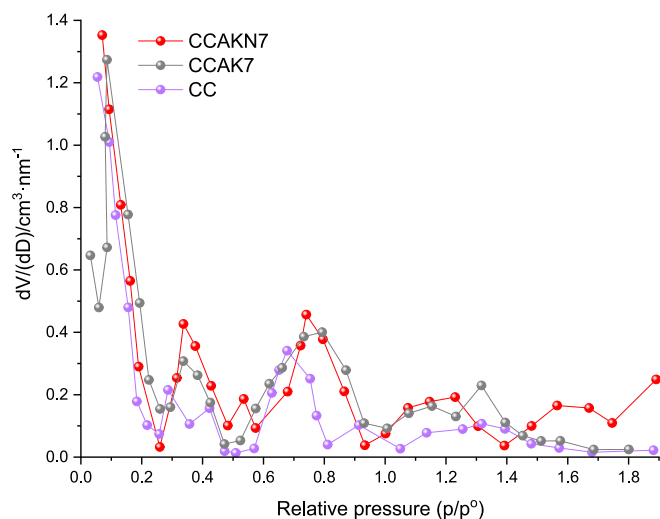


Fig. 7. The particle size distribution for the activated carbons.

On the other hand, immersion calorimetry measurements were carried out with different molecules with 0 dipole moments for the three activated carbons prepared from maize gopher. Fig. 8 shows the results obtained when the immersion calorimetry was carried out with the following probe molecules in the CCAKN7 activated carbon: dichloromethane (DCM) 0.33 nm, benzene (B.Z.) 0.37 nm, acetone 0.47 nm, cyclohexane 0.54 nm, 2,2-dimethylbutane (DMB) 0.56 nm, benzene 0.59 nm, Carbon Tetrachloride (CTC) 0.60 nm, toluene 0.61 nm, ethylbenzene 0.67 nm, α -pinene 0.70 nm, *meta*-xylene 0.71 nm, *ortho*-xylene 0.74 nm, Tri 2,4-polyphosphate 1.5 nm. The same experiments are carried out for the CCAK7 and CC activated carbon, and the same trends are obtained. Analyzing the graph showing the immersion enthalpies as a function of the diameter of each probe molecule and comparing it with the PSD shown in Fig. 5c, it can be observed that in the range of 0.30 nm and 0.45 nm, there is a slight increase in immersion enthalpy and then a decrease, a trend that is the same as that observed in the PSD calculated using the QSDFT kernel. Denoyel et al. analyzed this type of behavior using activated carbons (Rouquerol et al., 1989), they discussed how the surface of the carbons is accessible to the molecules they used based on the molecular size of the immersed liquids. In this study, the results of the direct comparison of the immersion enthalpy as a function of the kinetic diameter of each molecule show that for the

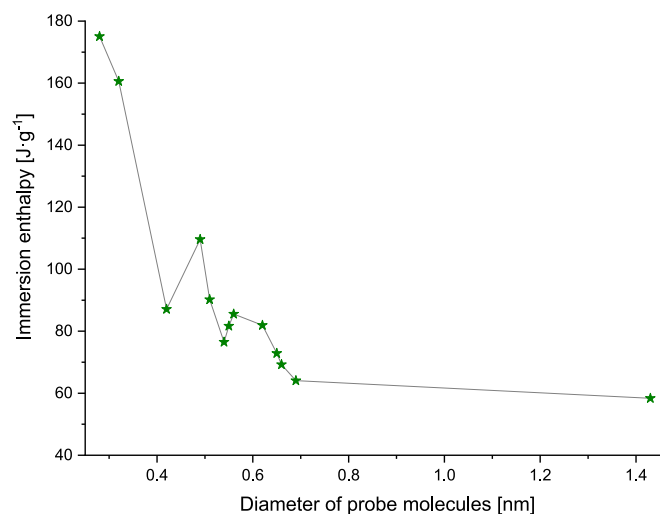


Fig. 8. The immersion enthalpies were plotted against the kinetic diameter of probe molecules.

activated carbon prepared, this first zone is as we have mentioned in the previous paragraph.

In zone 2, between 0.45 nm and 0.75 nm, we can see that the enthalpy values increase and decrease according to the probe molecule, which allows the heat of immersion to be related to the diffusion of the molecule size. In this same zone, with the probe molecules used in this study and the molecular diameters shown, the PSDs evaluated with the QSDFT kernel have an acceptable similarity with the zone of immersion enthalpies.

Zone 3, as defined in this work, is found at values greater than 0.75 nm. Comparing Fig. 5c and 5d and considering that only one probe molecule was used in this zone (Tri 2,4-polyphosphate 1.5 nm), the results of the enthalpy plot do not show a follow-up of the s PSD. This means that calorimetry experiments must be performed on molecules with different molecular diameters and a dipole moment equal to 0. However, in general, considering the results obtained in this investigation, it can be stated that the immersion calorimetry, under the experimental conditions used in this work, can be used as an analytical tool to study the pore size distribution for the prepared activated carbon.

3.6. Uranium adsorption isotherms

When investigating adsorption phenomena in the aqueous phase, it becomes essential to conduct thermodynamic analyses. These investigations aid in assessing the viability of the adsorption process and understanding the influence of temperature on these interactions. In the context of this study, the following thermodynamic parameters were computed: the variation in standard Gibbs free energy (ΔG°), standard enthalpy (ΔH°), and standard entropy (ΔS°). Furthermore, the outcomes derived from the aqueous solutions were subjected to evaluation through established models from specialized literature. This meticulous examination facilitated the assessment of the equilibrium achieved within the adsorbate-adsorbent system, thereby determining the maximum capacity for adsorbate adsorption (CC, CCAK7, and CCAKN7 in this instance).

Numerous models found in the specialized literature serve as valuable tools for approaching this type of investigation. The models formulated by Langmuir (Langmuir, 1916) and Freundlich (Proctor and Toro-Vazquez, 1996) have gained substantial traction in such research endeavors. These models effectively describe the equilibrium existing between the liquid and solid phases. Notably, these models characterize adsorption isotherms using a pair of parameters. Conversely, certain models portray equilibrium in both the liquid and solid phases while employing a greater number of parameters. Notably, the Sips model stands out among such approaches, encompassing three parameters to represent the adsorption isotherm (Guo et al., 2011). This extended parameterization can offer a deeper understanding of the adsorption process compared to the simpler two-parameter isotherm models.

3.6.1. Langmuir model

The Langmuir model postulates adsorption on a surface containing uniform energetic sites. In this scenario, each adsorbate molecule takes up a single adsorption site, and the highest level of adsorption corresponds to the creation of a complete monolayer. Importantly, in this state, adsorbate molecules do not diffuse across the adsorbent surface (Kumar et al., 2024). The mathematical representation of the Langmuir isotherm model is given by equation (3):

$$q_e = \frac{q_m K_L C_e}{1 + K_L C_e} \quad (3)$$

where q_m (mg.g^{-1}) is the maximum adsorption capacity of the adsorbent, K_L (L.mg^{-1}) is the Langmuir equilibrium constant, which is related to the biosorption energy.

3.6.2. Freundlich model

The Freundlich isotherm model is reported in equation (4):

$$qe = K_F C_e^{1/n_F} \quad (4)$$

The equilibrium adsorption capacity of U(VI) onto the prepared activated carbons (CCA7, CCAKN7, and CC) is denoted as q_e ($\text{mg}\cdot\text{g}^{-1}$), while the concentration of U(VI) at equilibrium is represented by C_e ($\text{mg}\cdot\text{L}^{-1}$). The parameter K_F ($\text{mg}\cdot\text{g}^{-1} (\text{L}\cdot\text{mg}^{-1})^{1/n_F}$) along with n_F corresponds to the constants of the Freundlich isotherm, which are linked to the adsorption capacity and intensity, respectively. The Freundlich constant (n_F) is indicative of the adsorption capacity and serves as a measure of the favorability of the adsorption process. Specifically, n_F values ranging between 2 and 10 suggest a substantial adsorption capacity, while values between 1 and 2 denote a moderate adsorption capacity. Values below 1 indicate a limited adsorption capacity (Proctor and Toro-Vazquez, 1996).

3.6.3. Sips model (Langmuir-Freundlich)

The two previous isothermal models have been widely used to analyze adsorption processes, especially in the aqueous phase. The Sips model incorporates both the Freundlich and Langmuir models and, as mentioned in the previous paragraph, has three parameters derived from the theory of these models (de Vargas Brião et al., 2023). It has a higher probability of describing the adsorption capacity of a system in equilibrium during adsorption. The Sips isotherm model (also known as Langmuir-Freundlich equation) is expressed by equation (5) below:

$$qe = \frac{q_{s,max}(K_s C_e)^{1/n_s}}{1 + (K_s C_e)^{1/n_s}} \quad (5)$$

where q_e ($\text{mg}\cdot\text{g}^{-1}$) and C_e ($\text{mg}\cdot\text{L}^{-1}$) correspond to the equilibrium adsorption capacity of the adsorbate per unit mass of the adsorbent and the equilibrium concentration of the adsorbate. On the other hand, $q_{s,max}$ ($\text{mg}\cdot\text{g}^{-1}$) describe the maximum adsorption capacity calculated from the Sips isotherm, k_s ($\text{mL}\cdot\text{mg}^{-1}$), and n_s are the Sips constants.

n_s corresponds to a factor associated with heterogeneity; a value of n_s close to or equal to 1 occurs in adsorbents with homogeneous active sites, while n_s values close to 0 correspond to adsorbents with heterogeneous active sites (Kumar et al., 2024). The adsorption equilibrium isotherms are shown in Fig. 9, and the model constants are tabulated in Table S1.

Furthermore, uncertainty studies were conducted to assess the reproducibility and reliability of the measurements. All repeated cycles, up to five measurements for each sample, demonstrated remarkable consistency, with deviations consistently within the range of $\pm 3\%$. This high level of precision underscores the reliability of the experimental approach and the reproducibility of the adsorption performance of the activated carbon samples. Such uncertainty analysis is crucial for validating the applicability of the materials in adsorption studies and provides confidence in the accuracy of the isotherm data presented.

Based on the data outlined in Table S1, it is evident that the Sips model offers a superior representation of uranium ion adsorption onto

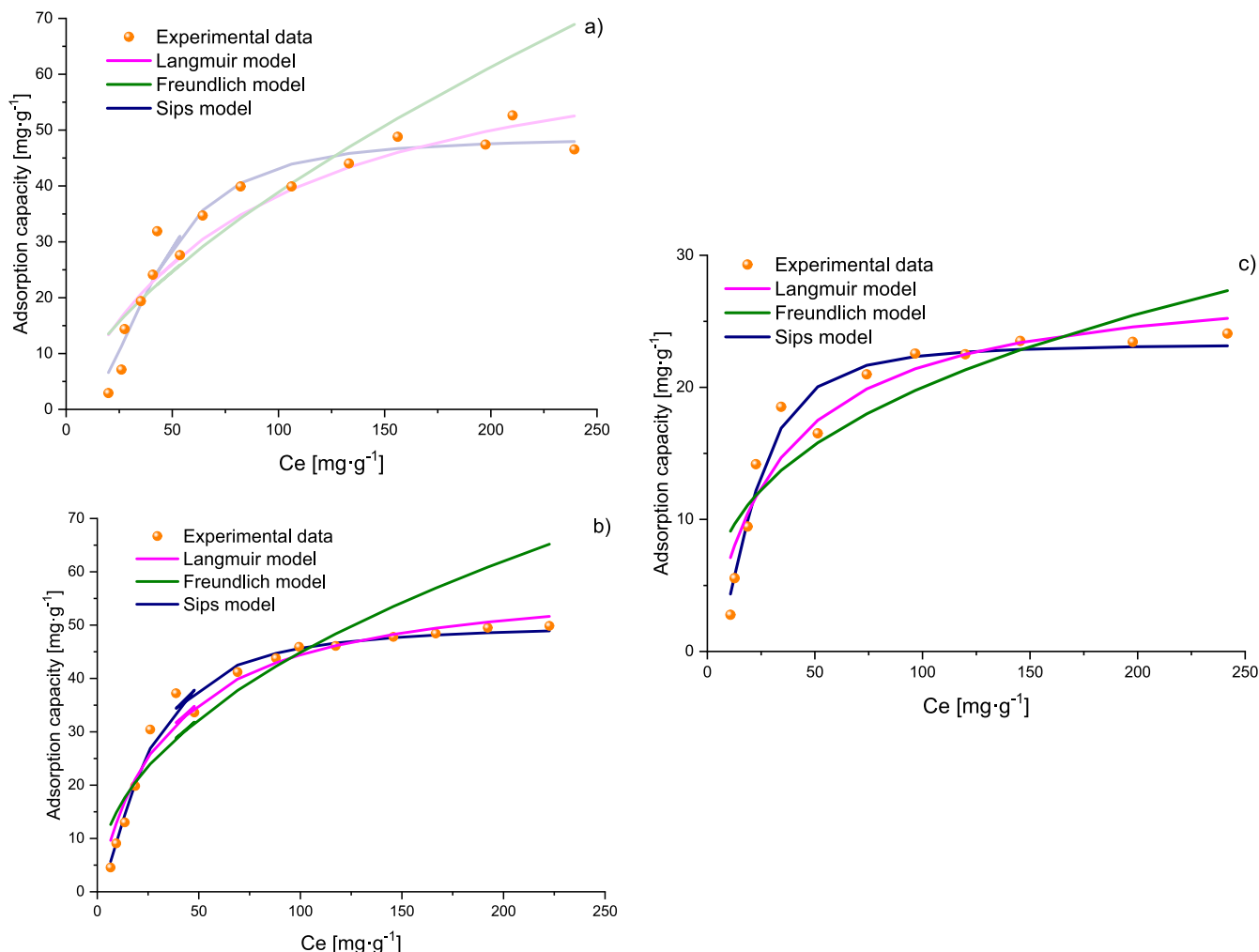


Fig. 9. Adsorption isotherms of uranium on activated carbons prepared from corncob a) CCAKN7 b) CCA7 c) CC (C_e : 100 ppm; pH 6.00; T: 298 K).

activated carbon samples compared to the Langmuir and Freundlich models (Kumar et al., 2024; Gieroba et al., 2023). This assertion is substantiated when scrutinizing the R^2 values obtained. It is pertinent to recall that the Sips model amalgamates elements of the Langmuir and Freundlich models, rendering it particularly valuable due to its ability to accommodate adsorption on diverse and heterogeneous adsorbent surfaces. Notably, the Sips model effectively circumvents the limitation observed in the Freundlich isotherm model, which arises during escalated adsorbate concentrations. See (Fig. 10).

The adaptability of the Sips model is evidenced in its transformation from the Freundlich isotherm at low adsorbate concentrations to the Langmuir isotherm at elevated concentrations. Insight from Fig. 9 reveals a convergence towards a Freundlich isotherm behavior for the three adsorbents employed at low uranium concentrations (Foo and Hameed, 2010). Conversely, as the uranium molecule concentration increases, the Langmuir isotherm's characteristic attributes manifest, indicating adsorption saturation. In this investigation, the maximal adsorption capacities registered were 51.66, 46.32, and 22.12 $\text{mg}\cdot\text{g}^{-1}$ for CCAKN7, CCAK7, and CC, respectively, specifically at a temperature of 298 K (the adsorptions at other temperatures are delineated in Table S1). Within the framework of the Sips model, the parameter n_s signifies the extent of surface heterogeneity. The obtained n_s values provide insight into the heterogeneous nature of the adsorbents' surfaces, which, notably, foster favorable conditions for the adsorption of U (VI) onto the meticulously prepared activated carbons.

3.7. U(VI) adsorption kinetics on CCAKN7, CCAK7, and CC samples

The effect of time during the uranium adsorption process on the activated carbon prepared in this work was studied using five different concentrations – from 20 to 100 ppm – (also at four different temperatures). The results of the adsorption capacity versus time obtained in this investigation for each of the samples of adsorbents produced varied with time. The results showed that the activated carbon that showed a higher rate of U(VI) adsorption at the different temperatures studied was the one activated with urea (CCAKN7). Kinetic results showed that uranium adsorption on the CCAKN7 sample increased rapidly during the first minutes to reach saturation, which occurred after approximately 55 min. When reviewing the specialized literature, it was found that other types of adsorbent materials have been used to remove uranium. Still, these materials generally present longer adsorption times, which gives the coals prepared in this study from gopher maize, under the

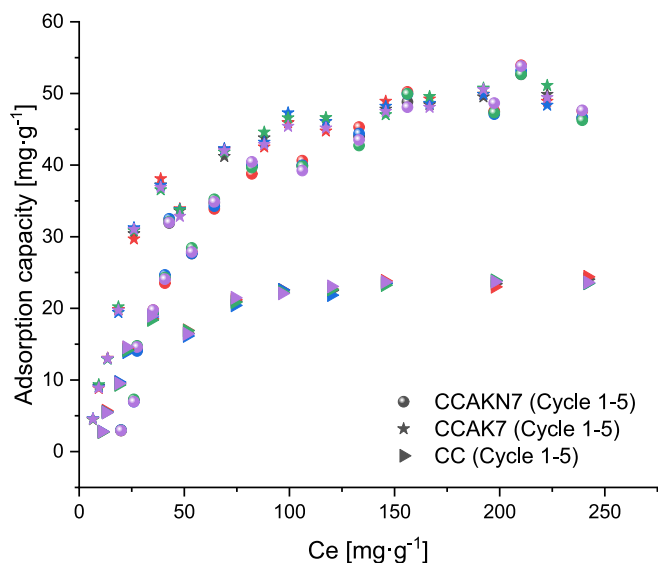


Fig. 10. Adsorption Isotherms of uranium on CCAKN7, CCAK7, CC (Co: 100 ppm; pH 6.00; T: 298 K).

parameters used in the laboratory, an additional plus for the use of these materials as regards applicability in the field of eliminating this undesirable radioactive compound. The results of the kinetic study showed that as time passed in each experiment, the adsorption sites on the surface of each activated carbon decreased because they were occupied by uranium until they reached the saturation point, which is why it is observed that the rate of adsorption decreases and slowly falls to zero, reaching a dynamic equilibrium (Shah et al., 2016; Delval et al., 2002; Undabeytia et al., 2002; Li et al., 2005; Carneiro et al., 2015; Motekaitis and Martell, 1985). Thus, the uranium adsorption capacity is a function of each activated carbon's structural characteristics, surface chemistry, and temperature variation (Xie et al., 2011).

Therefore, to determine the step that limits the adsorption rate of U (VI) transport from the liquid phase on each of the prepared activated carbons, i.e., to study in detail the adsorption mechanism for the uranium-activated carbon system, a detailed kinetic study was carried out. The pseudo-first-order (Lagergren, 1898) and pseudo-second-order (Ho, 1995) kinetic models are the most commonly used for this type of study. The Elovich models (Elovich and Larinov, 1962) and the kinetic intra-particle diffusion model (Inoue et al., 2004) have also been used.

The pseudo-first order and the pseudo-second order equations are generally expressed as equations (6) and (7), respectively, as follows:

$$\text{Log}(q_e - q_t) = \text{Log}(q_e) - \frac{K_1}{2,303} t \quad (6)$$

where q_e and q_t are the equilibrium adsorption capacities (mg/g), t is a given equilibrium time (min), and K_1 is the pseudo-first-order adsorption constant (min^{-1}).

$$\frac{t}{q_t} = \frac{1}{K_2 q_e^2} + \frac{1}{q_e} t \quad (7)$$

where q_t is the amount adsorbed (mg/g) at a given time t (min), q_e is the amount adsorbed at equilibrium (mg/g), K_2 is the constant given by the equation ($\text{g}/\text{mg}\cdot\text{min}$), and to find the constants of the pseudo-second kinetic model, (t/q_t) vs (t) , where the intercept ($1/q_e$) and slope ($\frac{1}{K_2 q_e^2}$), give the theoretical equilibrium concentration to be compared with the initial q_e .

The empirical Elovich adsorption model, widely applicable to many adsorption systems, was also applied to the results. This model assumes the energetic heterogeneity of adsorption sites in the form of a rectangular distribution (de Vargas Brião et al., 2023). The Elovich kinetic model is described by the equation (8):

$$q_t = \beta \ln(\alpha \beta + \beta \ln(t)) \quad (8)$$

where q_t ($\text{mg}\cdot\text{g}^{-1}$) is the adsorption capacity at time t , α is the initial adsorption rate from the Elovich equation ($\text{mg}\cdot\text{g}^{-1}\cdot\text{min}^{-1}$), and β is the desorption constant of the model ($\text{g}\cdot\text{mg}^{-1}$), which is related to the adsorption energy. The Elovich equation can be linearized assuming $\alpha \beta t \gg 1$ and that $q = 0$ at $t = 0$ and that $q = q_t$ for a time $t = t_t$. Under these conditions, a plot of q_t versus a $\ln(t)$ shows a linear relationship with a slope of $(1/\beta)$ and intercept $(1/\beta) \ln(\alpha \beta)$ (de Vargas Brião et al., 2023). This model was proposed to consider the kinetics of adsorption as a process that occurs in two phases: a rapid initial reaction associated with the movement of the adsorbate into the most accessible parts of the adsorbent, followed by a slower reaction due to diffusion of particles inside and outside the micropores of the adsorbent (Önal, 2006).

The intraparticle kinetic model is based on the theory of Weber and Morris (Weber and Morris, 1963), which represents the following variables: q_t , K_i , $t^{1/2}$. In the intraparticle model, the step that limits the adsorption of the adsorbate in the adsorbent is described according to the following equation (9):

$$q_t = K_i \cdot t^{1/2} + C \quad (9)$$

where C ($\text{mg}\cdot\text{g}^{-1}$) is an indicator of the thickness of the adsorption boundary layer, i.e. the greater the intercept, the greater the Effect of the

boundary layer and is evaluated by the intercept in the graph in its linearized form; K_i ($\text{mg}\cdot\text{g}^{-1}\cdot\text{min}^{-0.5}$) is the intraparticle diffusion rate constant and is obtained from the slope of the graph in its linearized form by plotting qt versus $t^{1/2}$.

The results obtained for each of the parameters of the kinetic models used in this research for each of the samples of activated carbons prepared from corncob are summarized in Table S2. Looking at the values obtained for R^2 (the criterion used to determine which of the kinetic models was the best fit) for each of the kinetic models studied in this research, to determine the U(VI) adsorption mechanism on the different activated carbons (CCAKN7, CCAK7 and CC), it can be concluded that the perturbation of the U(VI) adsorption mechanism on the different activated carbons (CCAKN7, CCAK7 and CC) was not significant. It can be concluded that the pseudo-second-order kinetic model is the one that best describes the U(VI) adsorption process under the conditions used in this study. Other authors have reported similar results using this molecule on other adsorbents (Khenifi et al., 2010; Cheung et al., 2007). This leads to the conclusion that the adsorption process is fundamentally controlled by a chemical reaction which is the main step and limits the rate in the whole adsorption process (Wu et al., 2005; Juang et al., 2000; Ho and McKay, 1998; Ho and McKay, 1999), in chemisorption.

In this study, along with the pseudo first-order, pseudo-second-order, and Elovich models, the intraparticle diffusion model, derived from Fick's Law, was also employed. This model offers valuable insights into the adsorbate's penetration into the adsorbent's pores. Pioneered by Weber and Morris, a notable finding is that if intraparticle diffusion

governs the rate, the adsorption onto the adsorbent changes proportionally to the square root of time (Delval et al., 2002). Consequently, in experiments of this nature, adsorption rates are gauged by associating the adsorbent's capacity with the square root of time (Carneiro et al., 2015; Motekaitis and Martell, 1985; Xie et al., 2011; Lagergren, 1898). It has been established that a plot of qt against \sqrt{t} must originate from the origin when intraparticle diffusion solely dictates the pace. Deviations from this origin point suggest the presence of a boundary layer control factor, indicating that other kinetic models also influence the rate-limiting steps alongside intraparticle diffusion. This is illustrated in Fig. 11, where the intraparticle diffusion model is applied to the activated carbons synthesized in this study at a concentration of $100\text{ mg}\cdot\text{L}^{-1}$. The diffusion process appears to transpire in two stages, with the slowest step predominantly governing the overall process velocity, aligning closely with chemical kinetics principles.

In batch experiments, intraparticle diffusion frequently acts as the rate-limiting step. Correlation coefficients for the intraparticle diffusion model are presented in Table S2, resembling those reported for the pseudo-second-order kinetics model. To summarize, when subjecting the intraparticle diffusion model to analysis, the behavior of the three activated carbon samples (CCAKN7, CCAK7, and CC) demonstrates consistency with this model. This is revealed by plotting experimental data (not displayed here). The interpretation is that the adsorption process transpires in two modes: a) superficial diffusion, and b) intraparticle diffusion (Undabeytia et al., 2002; Li et al., 2005). Furthermore, upon meticulous graph analysis, a slight curve emerges initially due to

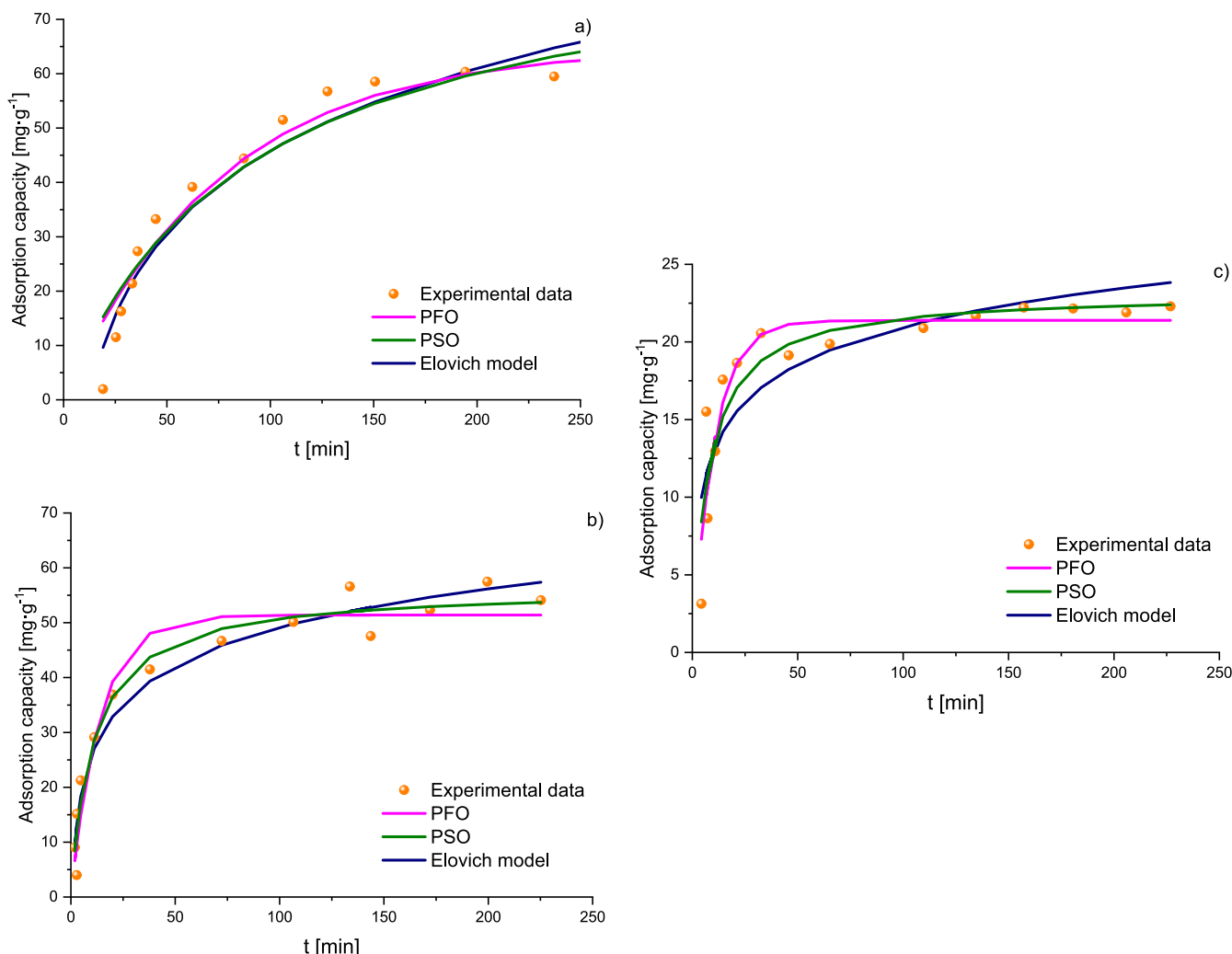


Fig. 11. Kinetic studies for the three activated carbons a) CCAKN7, b) CCAK7 and c) CC samples (at a concentration of $100\text{ mg}\cdot\text{L}^{-1}$).

the influence of the boundary layer, followed by a fully linear segment indicative of intraparticle diffusion or porosity. The slope of the second linear segment represents the intraparticle diffusion parameter K_i , while the point of intersection reflects the boundary layer's effect. A greater intersection signifies heightened contribution from surface adsorption in the rate-limiting stage. The K_i values computed for the intraparticle diffusion coefficient are outlined in Table S2 for CCAKN7, CCAK7, and CC carbons in the context of U(VI) adsorption. C signifies the intersection and pertains to the boundary layer's thickness. Notably, the value assumed by the constant is instrumental in result interpretation. Literature suggests that a high C value corresponds to an escalated boundary layer effect (Konicki et al., 2012). The plotted data, not originating from the origin ($C \neq 0$), indicates a certain level of boundary layer control during the approach of U(VI) molecules to the activated carbon. This signifies that intraparticle diffusion isn't the exclusive rate-limiting step for the three prepared adsorbents; multiple stages can concurrently influence the adsorption rate (Butt et al., 2023).

3.8. Thermodynamic studies

A study of the Effect of the temperature variable on U(VI) adsorption was carried out on each of the activated carbon samples prepared from corncob to carry out the thermodynamic study of uranium adsorption on the CCAKN7, CCAK7 and CC samples. The results obtained showed that the adsorption process is exothermic, and it is also feasible to calculate the thermodynamic parameters as the change of Gibbs free energy (ΔG°), enthalpy (ΔH°) and entropy (ΔS°) that can be calculated from Eqs. (10) and (13):

Thermodynamic parameters consisting of Gibbs free energy change (ΔG°), enthalpy change (ΔH°) and entropy change (ΔS°) were calculated from Eq:

$$\Delta G^\circ = -RT \ln K_L \quad (10)$$

where R is the universal gas constant ($8.314 \text{ J/mol.K}^{-1}$), T is the temperature (K), and the value of K_L was calculated using the following equation:

$$K_L = \frac{q_e}{C_e} \quad (11)$$

where q_e and C_e are the equilibrium concentration of glyphosate and activated carbon samples (mg.g^{-1}) in the aqueous solution (mg.L^{-1}), respectively. The enthalpy change (ΔH°) and entropy change (ΔS°) of adsorption were estimated from the following equation:

$$\ln K_L = \frac{\Delta S^\circ}{R} - \frac{\Delta H^\circ}{RT} \quad (12)$$

The enthalpy change (ΔH°) and entropy change (ΔS°) can be obtained from the slope and intercept from the Van't Hoff equation of (ΔG°) as follows:

$$\Delta G^\circ = \Delta H^\circ - T\Delta S^\circ \quad (13)$$

where ΔG° is the Gibbs free energy change (J), R is the universal gas constant ($8.314 \text{ J/mol. K}^{-1}$) and T is the absolute temperature (K).

The Gibbs free energy change (ΔG°) is the fundamental thermodynamic criterion for the spontaneity of a chemical reaction. In general, ΔG° is smaller in physisorption than in chemisorption. The free energy change for physisorption is in the range of 20 to 0 kJ/mol, physisorption together with chemisorption is in the range of 20 to 80 kJ/mol, and chemisorption is in the range of 80 to 400 kJ/mol (Kara et al., 2003; Diel et al., 2021).

According to the results obtained for each of the activated carbon prepared in this work, the ΔG° for the adsorption of U(VI) on each of the samples studied in this work is between the range -41.66 to $-21.32 \text{ kJmole}^{-1}$. Therefore, uranium adsorption on the activated carbons prepared from the corn gopher can be considered physical adsorption that is enhanced by an effect of a chemical nature. It is also observed that the U

(VI) adsorption process on activated carbon samples is exothermic, as the Gibbs free energy values decrease as a function of temperature. On the other hand, the magnitude of the enthalpy change values (ΔH°) also allows us to establish whether the process between the adsorbate-adsorbent interaction is of an exothermic or endothermic nature during the adsorption process studied in this investigation. This argument also allows us to establish whether the process is of the physisorption or chemisorption type. In the specialized literature, some authors (Inglezakis and Zorpas, 2012; Zou et al., 2023) have suggested that if the ΔH° is equivalent to the physisorption, its value should be lower than 40 kJ/mol (Kokalj, 2022). In this study, the following values were obtained for ΔH° for CCAKN 7, CCAK 7, and CC carbon: -94.65 kJ/mol , -65.34 kJ/mol and -52.81 kJ/mol , respectively, for U(VI) adsorption. Therefore, ΔH° , ΔG° , and ΔS° suggest the same fact: the adsorption of U(VI) ions on the three activated carbons prepared from corn gopher is carried out by a physical adsorption process, which is potentiated by a chemical type of Effect. The negative values obtained for ΔS° in the activated carbon samples can be interpreted as the result of the disturbance suffered by the system at the solid-liquid interface, which decreases during adsorption. Finally, the comparison of ΔH° with $T\Delta S^\circ$ shows that it is only ΔH° that is responsible for the negative values of ΔG° . Therefore, in this case, the adsorption process of U(VI) ions can be considered a process that is essentially controlled by the enthalpic thermodynamic variable.

A literature review has shown that some authors have similar thermodynamic results. On the other hand, the degree of freedom between the solid-liquid interface decreases during the adsorption process, and some structural changes occur in both the adsorbate and the adsorbent if the results obtained for ΔS° are appropriately interpreted. According to the theory corresponding to the exchange of adsorption from aqueous solution, for the adsorption process carried out by the exchange at the solid-liquid interface, the solute (U(VI)) migrates from the liquid phase to this interface. This causes the system to reduce its degrees of freedom (including translation and rotation). This can be explained by the fact that the entropy corresponding to the adsorption process is reduced. However, in the liquid phase, during the adsorption of U(VI), it is likely that it eventually generates a contraction in some pores of the activated carbon structure, causing some of the water on the surface of the adsorbents to become hydration water. and this process of desorption of the water molecule is responsible for the fact that the entropy of the process increases. It can, therefore, be concluded that the entropy value is a sum of these phenomena.

3.9. Eco-friendly recovery and reuse of uranium and adsorbents: A sustainable approach

For utilizing adsorbed uranium involves a combination of mild chemical treatments and sustainable practices. First, desorption of uranium can be achieved using biodegradable weak acids such as citric acid or acetic acid, which are less harmful to the environment compared to strong mineral acids like HCl or HNO₃. Alternatively, neutral salt solutions such as sodium chloride or sodium bicarbonate can be employed to induce desorption through ion exchange, minimizing the production of chemical waste. Once uranium is desorbed, it can be precipitated as a stable compound by adjusting the pH of the solution with a natural alkali such as lime (Ca(OH)₂). This process allows uranium to form compounds like uranium hydroxide or uranium phosphate, which can then be filtered and collected. The precipitated uranium can be calcined at moderate temperatures to convert it into uranium oxide, a stable solid form that is safe for long-term storage or suitable for reuse in nuclear fuel production. The recovered uranium oxide can be stored in secure, eco-friendly facilities for future use or provided to industries for applications such as isotope production or research, reducing the need for additional uranium mining. Meanwhile, the activated carbon used for uranium adsorption can be regenerated through thermal or chemical processes and reused for subsequent adsorption cycles, further

enhancing sustainability and reducing material waste. This method is highly eco-friendly as it employs biodegradable reagents, minimizes the use of hazardous chemicals, and avoids generating significant secondary waste. Additionally, it is cost-effective due to the use of inexpensive and readily available materials such as lime and mild acids, while enabling the repeated use of activated carbon. By focusing on the recovery and reuse of both uranium and the adsorbent, this approach aligns with the principles of green chemistry and a circular economy, ensuring minimal environmental impact and sustainable resource management.

4. Conclusion

This study successfully synthesized and characterized nitrogen-doped and KOH-activated carbons derived from corn cob biomass, demonstrating their potential as highly efficient adsorbents for uranium (VI) removal from aqueous solutions. The materials were prepared using chemical activation with KOH and nitrogen doping through urea impregnation, resulting in functionalized activated carbons with exceptional structural and chemical properties. Comprehensive characterization using thermogravimetric analysis (TGA), Fourier-transform infrared spectroscopy (FTIR), scanning electron microscopy (SEM), nitrogen adsorption isotherms, and immersion calorimetry provided detailed insights into the materials' hierarchical pore structure, thermal stability, and surface chemistry. The synthesized activated carbons exhibited hierarchical porosity with predominant micropores and a contribution from narrow mesopores, as confirmed by type Ib isotherms and H4 hysteresis loops. Among the samples, the nitrogen-doped carbon (CCAKN7) demonstrated the highest BET surface area (1395 m²/g), followed by CCAK7 (915 m²/g) and CC (563 m²/g). Pore size distribution analysis highlighted the effectiveness of the activation processes, with nitrogen doping further enhancing the micropore and mesopore development. FTIR spectroscopy identified nitrogen-containing functional groups, such as amines and pyridinic nitrogen, which significantly improved the materials' chemical reactivity and adsorption affinity for U(VI). Adsorption studies revealed that the nitrogen-doped activated carbon (CCAKN7) exhibited the highest uranium (VI) adsorption capacity at 51.66 mg/g, followed by CCAK7 (46.32 mg/g) and CC (22.12 mg/g). The adsorption behavior was best described by the Sips isotherm model, indicating a heterogeneous adsorption surface and favorable interactions between the adsorbents and uranium ions. Adsorption kinetics followed a pseudo-second-order model, confirming that chemisorption was the dominant mechanism, and equilibrium was achieved rapidly within 55 min. These findings underscore the efficiency and practical applicability of these materials for uranium adsorption. Thermodynamic analyses further confirmed that uranium adsorption onto the activated carbons was both spontaneous and exothermic, as evidenced by negative Gibbs free energy (ΔG°), enthalpy (ΔH°), and entropy (ΔS°) values. The variations in these thermodynamic parameters among the samples highlighted the influence of chemical activation and nitrogen doping on the adsorption energetics and material properties. The incorporation of nitrogen into the carbon framework not only improved adsorption performance but also enhanced the thermal stability and structural robustness of the materials, as revealed by TGA analysis. The results of this study demonstrate that nitrogen-doped activated carbons derived from renewable corn cob biomass are cost-effective, sustainable, and efficient adsorbents for U(VI) removal. Their high surface area, hierarchical pore structure, and enhanced surface functionality make them suitable for environmental remediation and nuclear waste management. Furthermore, the structural and functional characteristics of these materials suggest their potential applicability for the adsorption of other heavy metals and contaminants. This research underscores the transformative potential of renewable biomass-derived materials in addressing global environmental challenges while promoting sustainability and resource efficiency.

CRedit authorship contribution statement

Liliana Giraldo: Writing – original draft, Supervision, Methodology, Investigation, Formal analysis, Data curation, Conceptualization. **Jaroslław Serafin:** Writing – review & editing, Writing – original draft, Visualization, Validation, Supervision, Project administration, Methodology, Investigation, Formal analysis, Data curation, Conceptualization. **Bartosz Dziejarski:** Data curation, Formal analysis, Validation, Writing – review & editing, Visualization. **Juan Carlos Moreno-Piraján:** Writing – original draft, Supervision, Methodology, Investigation, Formal analysis, Data curation, Conceptualization.

Declaration of competing interest

The authors declare that they have no known competing financial interests or personal relationships that could have appeared to influence the work reported in this paper.

Acknowledgments

The authors also thank the framework agreement between Universidad Nacional de Colombia and Universidad de los Andes (Bogotá, Colombia) under which this work was carried out. Professor Juan Carlos Moreno-Piraján also thanks for the grant to the Facultad de Ciencias of Universidad de los Andes, number INV-2023-1622735. Jaroslław Serafin is grateful to Professor Juan Carlos Moreno-Piraján and Universidad de los Andes for the opportunity to carry out this research.

Appendix A. Supplementary data

Supplementary data to this article can be found online at <https://doi.org/10.1016/j.ces.2025.121222>.

Data availability

Data will be made available on request.

References

- Anirudhan, T.S., Divya, L., Suchithra, P.S., 2009. Kinetic and equilibrium characterization of uranium (VI) adsorption onto carboxylate-functionalized poly (hydroxyethylmethacrylate)-grafted lignocellulosics. *J. Environ. Manage.* 90 (1), 549–560.
- Barker-Rothschild, D., Chen, J., Wan, Z., Rennecker, S., Burgert, I., Ding, Y., Rojas, O.J., 2025. Lignin-based porous carbon adsorbents for CO₂ capture. *Chem. Soc. Rev.*
- Basak, B., Kumar, R., Bharadwaj, A.S., Kim, T.H., Kim, J.R., Jang, M., Jeon, B.H., 2023. Advances in physicochemical pretreatment strategies for lignocellulosic biomass and their effectiveness in bioconversion for biofuel production. *Bioresour. Technol.* 369, 128413.
- Bayramoğlu, G., Çelik, G., Arica, M.Y., 2006. Studies on accumulation of uranium by fungus *Lentinus sajor-caju*. *J. Hazard. Mater.* 136 (2), 345–353.
- Bharadwaj, A.S., Dev, S., Zhuang, J., Wang, Y., Yoo, C.G., Jeon, B.H., Kim, T.H., 2023. Review of chemical pretreatment of lignocellulosic biomass using low-liquid and low-chemical catalysts for effective bioconversion. *Bioresour. Technol.* 368, 128339.
- Brunauer, S., Emmett, P.H., Teller, E., 1938. Adsorption of gases in multimolecular layers. *J. Am. Chem. Soc.* 60 (2), 309–319.
- Burns, P.C., Ewing, R.C., Navrotsky, A., 2012. Nuclear fuel in a reactor accident. *Science* 335 (6073), 1184–1188.
- Butt, H.J., Graf, K., Kappel, M., 2023. *Physics and chemistry of interfaces*. John Wiley & Sons.
- Carneiro, R.T., Taketa, T.B., Neto, R.J.G., Oliveira, J.L., Campos, E.V., de Moraes, M.A., Fraceto, L.F., 2015. Removal of glyphosate herbicide from water using biopolymer membranes. *J. Environ. Manage.* 151, 353–360.
- Carrott, P.J.M., Carrott, M.R., 1999. Evaluation of the Stoeckli method for the estimation of micropore size distributions of activated charcoal cloths. *Carbon* 37 (4), 647–656.
- Chardi, K.J., Satpathy, A., Schenkeveld, W.D., Kumar, N., Noël, V., Kraemer, S.M., Giammar, D.E., 2022. Ligand-induced U mobilization from chemogenic uraninite and biogenic noncrystalline U (IV) under anoxic conditions. *Environ. Sci. Tech.* 56 (10), 6369–6379.
- Chen, T., Shi, P., Zhang, J., Li, Y., Duan, T., Dai, L., Zhu, W., 2018. Natural polymer konjac glucomannan mediated assembly of graphene oxide as versatile sponges for water pollution control. *Carbohydr. Polym.* 202, 425–433.

- Cheng, W., Ding, C., Sun, Y., Wang, X., 2015. Fabrication of fungus/attapulgite composites and their removal of U (VI) from aqueous solution. *Chem. Eng. J.* 269, 1–8.
- Cheung, W.H., Szeto, Y.S., McKay, G., 2007. Intraparticle diffusion processes during acid dye adsorption onto chitosan. *Bioresour. Technol.* 98 (15), 2897–2904.
- Choi, A.E.S., Futralan, C.C.M., Yee, J.J., 2020. Fuzzy optimization for the removal of uranium from mine water using batch electrocoagulation: a case study. *Nucl. Eng. Technol.* 52 (7), 1471–1480.
- Corner, A., Venables, D., Spence, A., Poortinga, W., Demski, C., Pidgeon, N., 2011. Nuclear power, climate change and energy security: exploring British public attitudes. *Energy Policy* 39 (9), 4823–4833.
- de Vargas Brião, G., Hashim, M.A., Chu, K.H., 2023. The Sips isotherm equation: Often used and sometimes misused. *Sep. Sci. Technol.* 58 (5), 884–892.
- Delval, F., Crini, G., Morin, N., Vebrel, J., Bertini, S., Torri, G., 2002. The sorption of several types of dye on crosslinked polysaccharides derivatives. *Dyes Pigm.* 53 (1), 79–92.
- Diel, J.C., Franco, D.S., Nunes, I.D.S., Pereira, H.A., Moreira, K.S., Burgo, T.A.D.L., Dotto, G.L., 2021. Carbon nanotubes impregnated with metallic nanoparticles and their application as an adsorbent for the glyphosate removal in an aqueous matrix. *J. Environ. Chem. Eng.* 9 (2), 105178.
- Ding, C., Cheng, W., Sun, Y., Wang, X., 2015. Novel fungus-Fe₃O₄ bio-nanocomposites as high performance adsorbents for the removal of radionuclides. *J. Hazard. Mater.* 295, 127–137.
- Dong, K., Sun, R., Jiang, H., Zeng, X., 2018. CO₂ emissions, economic growth, and the environmental Kuznets curve in China: what roles can nuclear energy and renewable energy play? *J. Clean. Prod.* 196, 51–63.
- Donohue, M.D., Aranovich, G.L., 1998. Adsorption hysteresis in porous solids. *J. Colloid Interface Sci.* 205 (1), 121–130.
- Dubrawski, K.L., van Genuchten, C.M., Delaire, C., Amrose, S.E., Gadgil, A.J., Mohseni, M., 2015. Production and transformation of mixed-valent nanoparticles generated by Fe (0) electrocoagulation. *Environ. Sci. Tech.* 49 (4), 2171–2179.
- Elovich, S.Y., Larinov, O.G., 1962. Theory of adsorption from solutions of non electrolytes on solid (I) equation adsorption from solutions and the analysis of its simplest form, (II) derivation of the equation of adsorption isotherm from solutions. *Izv. Akad. Nauk. SSSR, Otd. Khim. Nauk* 2 (2), 209–216.
- Fan, M., Wang, X.E., Song, Q., Zhang, L., Ren, B., Yang, X., 2021. Review of biomass-based materials for uranium adsorption. *J. Radioanal. Nucl. Chem.* 1–14.
- Foo, K.Y., Hameed, B.H., 2010. Insights into the modeling of adsorption isotherm systems. *Chem. Eng. J.* 156 (1), 2–10.
- Gan, J., Zhang, L., Wang, Q., Xin, Q., Hu, E., Lei, Z., Wang, H., 2023. Synergistic action of multiple functional groups enhanced uranium extraction from seawater of porous phosphorylated chitosan/coal-based activated carbon composite sponge. *Desalination* 545, 116154.
- Gandhi, T.P., Sampath, P.V., Maliyekkal, S.M., 2022. A critical review of uranium contamination in groundwater: treatment and sludge disposal. *Sci. Total Environ.* 825, 153947.
- Gani, A., Naruse, I., 2007. Effect of cellulose and lignin content on pyrolysis and combustion characteristics for several types of biomass. *Renew. Energy* 32 (4), 649–661.
- Ge, S., Wei, K., Peng, W., Huang, R., Akinlabi, E., Xia, H., Jiang, J., 2024. A comprehensive review of covalent organic frameworks (COFs) and their derivatives in environmental pollution control. *Chem. Soc. Rev.*
- Ghahri, S., Park, B.D., 2023. Ether bond formation in waste biomass-derived, value-added technical hardwood kraft lignin using glycolic acid. *Journal of Research Updates in Polymer Science* 12, 171–179.
- Gieroba, B., Kalisz, G., Krysa, M., Khalavka, M., Przekora, A., 2023. Application of vibrational spectroscopic techniques in the study of the natural polysaccharides and their cross-linking process. *Int. J. Mol. Sci.* 24 (3), 2630.
- Guo, L., Li, G., Liu, J., Ma, S., Zhang, J., 2011. Kinetic and equilibrium studies on adsorptive removal of toluidine blue by water-insoluble starch sulfate. *J. Chem. Eng. Data* 56 (5), 1875–1881.
- He, D., Wang, Q., Mu, J., 2024. Conversion of waste cork to N-doped porous carbons by urea-assisted hydrothermal method for enhanced VOC capture. *Waste Manag.* 175, 191–203.
- Hernowo, P., Steven, S., Maulidin, M., Arumsari, A.G., Bindar, Y., Syauket, A., Rukmayadi, D., 2024. Thermokinetic study of coconut husk pyrolysis in the devolatilization zone using volatile state approach. *Biomass Convers. Biorefin.* 1–15.
- Ho, Y.S., 1995. Absorption of heavy metals from waste streams by peat. University of Birmingham. Doctoral dissertation.
- Ho, Y.S., McKay, G., 1998. Sorption of dye from aqueous solution by peat. *Chem. Eng. J.* 70 (2), 115–124.
- Ho, Y.S., McKay, G., 1999. Pseudo-second order model for sorption processes. *Process Biochem.* 34 (5), 451–465.
- Hu, H., Jiang, B., Wu, H., Zhang, J., Chen, X., 2016. Bamboo (*Acidosasa edulis*) shoot shell biochar: Its potential isolation and mechanism to perhenate as a chemical surrogate for pertechnetate. *J. Environ. Radioact.* 165, 39–46.
- Huang, Z.W., Li, Z.J., Wu, Q.Y., Zheng, L.R., Zhou, L.M., Chai, Z.F., Shi, W.Q., 2018. Simultaneous elimination of cationic uranium (VI) and anionic rhodium (VII) by graphene oxide-poly (ethyleneimine) macrostructures: a batch, XPS, EXAFS, and DFT combined study. *Environ. Sci. Nano* 5 (9), 2077–2087.
- Huang, C.P., Wu, J.Y., Li, Y.J., 2018. Treatment of spent nuclear fuel debris contaminated water in the Taiwan Research Reactor spent fuel pool. *Prog. Nucl. Energy* 108, 26–33.
- Inglezakis, V.J., Zorpas, A.A., 2012. Heat of adsorption, adsorption energy and activation energy in adsorption and ion exchange systems. *Desalin. Water Treat.* 39 (1–3), 149–157.
- Inoue, M.H., Oliveira Jr, R.S., Regitano, J.B., Tormena, C.A., Constantin, J., Tornisielo, V. L., 2004. Sorption kinetics of atrazine and diuron in soils from southern Brazil. *J. Environ. Sci. Health B* 39 (4), 589–601.
- Jin, J., Li, S., Peng, X., Liu, W., Zhang, C., Yang, Y., Wang, X., 2018. HNO₃ modified biochars for uranium (VI) removal from aqueous solution. *Bioresour. Technol.* 256, 247–253.
- Juang, R.S., Wu, F.C., Tseng, R.L., 2000. Mechanism of adsorption of dyes and phenols from water using activated carbons prepared from plum kernels. *J. Colloid Interface Sci.* 227 (2), 437–444.
- Kara, M., Yuzer, H., Sabah, E., Celik, M.S., 2003. Adsorption of cobalt from aqueous solutions onto sepiolite. *Water Res.* 37 (1), 224–232.
- Khenifi, A., Derriche, Z., Mousty, C., Prévot, V., Forano, C., 2010. Adsorption of glyphosate and glufosinate by Ni₂Al₂O₇ layered double hydroxide. *Appl. Clay Sci.* 47 (3–4), 362–371.
- Kim, T.H., Park, S.H., Lee, S., Bharadwaj, A.S., Lee, Y.S., Yoo, C.G., Kim, T.H., 2023. A review of biomass-derived UV-shielding materials for bio-composites. *Energies* 16 (5), 2231.
- Kokalj, A., 2022. Corrosion inhibitors: physisorbed or chemisorbed? *Corros. Sci.* 196, 109939.
- Konicki, W., Petech, I., Mijowska, E., Jasińska, I., 2012. Adsorption of anionic dye Direct Red 23 onto magnetic multi-walled carbon nanotubes-Fe₃C nanocomposite: Kinetics, equilibrium and thermodynamics. *Chem. Eng. J.* 210, 87–95.
- Kumar, S., Loganathan, V.A., Gupta, R.B., Barnett, M.O., 2011. An assessment of U (VI) removal from groundwater using biochar produced from hydrothermal carbonization. *J. Environ. Manage.* 92 (10), 2504–2512.
- Kumar, K., Tyagi, U., Maity, S.K., Singh, S., 2024. A strategic approach towards the synthesis of jackfruit peel-based activated carbon. In: *Assessment of Different Activating Agents and Operating Conditions. Biomass Conversion and Biorefinery*, pp. 1–22.
- Lagergren, S., 1898. About the theory of so-called adsorption of soluble substances. *Langmuir*, 1916. The constitution and fundamental properties of solids and liquids. Part I. Solids *J. Am. Chem. Soc.* 38 (11), 2221–2295.
- Lei, J., Liu, H., Zhou, L., Wang, Y., Yu, K., Zhu, H., Zhu, W., 2023. Progress and perspective in enrichment and separation of radionuclide uranium by biomass functional materials. *Chem. Eng. J.*, 144586
- Li, B., Dai, F., Xiao, Q., Yang, L., Shen, J., Zhang, C., Cai, M., 2016. Nitrogen-doped activated carbon for a high energy hybrid supercapacitor. *Energ. Environ. Sci.* 9 (1), 102–106.
- Li, Z., Kruk, M., Jaroniec, M., Ryu, S.K., 1998. Characterization of structural and surface properties of activated carbon fibers. *J. Colloid Interface Sci.* 204 (1), 151–156.
- Li, T., Lin, X., Zhang, Z., Yang, L., Qian, Y., Fu, L., Wen, L., 2023. Photothermal-enhanced uranium extraction from seawater: a biomass solar thermal collector with 3D ion-transport networks. *Adv. Funct. Mater.* 33 (19), 2212819.
- Li, F., Wang, Y., Yang, Q., Evans, D.G., Forano, C., Duan, X., 2005. Study on adsorption of glyphosate (N-phosphonomethyl glycine) pesticide on MgAl-layered double hydroxides in aqueous solution. *J. Hazard. Mater.* 125 (1–3), 89–95.
- Li, P., Zhun, B., Wang, X., Liao, P., Wang, G., Wang, L., Zhang, W., 2017. Highly efficient interception and precipitation of uranium (VI) from aqueous solution by iron-electrocoagulation combined with cooperative chelation by organic ligands. *Environ. Sci. Tech.* 51 (24), 14368–14378.
- López-Francés, A., Cabrero-Antonino, M., Bernat-Quesada, F., Ferrer, B., Blanes, M., García, R., Navalón, S., 2024. Valorization of field-spent granular activated carbon as heterogeneous ozonation catalyst for water treatment. *ChemSusChem*, e202400062.
- Ma, H., Hsiao, B.S., Chu, B., 2012. Ultrafine cellulose nanofibers as efficient adsorbents for removal of UO₂²⁺ in water. *ACS Macro Lett.* 1 (1), 213–216.
- Ma, J., Ye, Z., Zhou, J., Hu, Z.T., Wang, Q., Wang, J., Hu, M., 2024. Co-pyrolysis of soybean straw and spirulina platensis for N-containing chemicals and N-doped carbon materials production: unraveling the nitrogen migration mechanism and involved chemical reactions. *J. Anal. Appl. Pyrol.* 181, 106641.
- Michot, L.J., Villieras, F., 2006. Surface area and porosity. *Developments in Clay Science* 1, 965–978.
- Motekaitis, R.J., Martell, A.E., 1985. Metal chelate formation by N-phosphonomethylglycine and related ligands. *J. Coord. Chem.* 14 (2), 139–149.
- Nariyan, E., Sillanpää, M., Wolkersdorfer, C., 2018. Uranium removal from Pyhäsalmi/Finland mine water by batch electrocoagulation and optimization with the response surface methodology. *Sep. Purif. Technol.* 193, 386–397.
- Neimark, A.V., Lin, Y., Ravikovitch, P.I., Thommes, M., 2009. Quenched solid density functional theory and pore size analysis of micro-mesoporous carbons. *Carbon* 47 (7), 1617–1628.
- Olivier, J.P., 1998. Improving the models used for calculating the size distribution of micropore volume of activated carbons from adsorption data. *Carbon* 36 (10), 1469–1472.
- Önal, Y., 2006. Kinetics of adsorption of dyes from aqueous solution using activated carbon prepared from waste apricot. *J. Hazard. Mater.* 137 (3), 1719–1728.
- Park, S.J., Jung, W.Y., 2003. KOH activation and characterization of glass fibers-supported phenolic resin. *J. Colloid Interface Sci.* 265 (2), 245–250.
- Proctor, A.U.O.A., Toro-Vazquez, J.F., 1996. The Freundlich isotherm in studying adsorption in oil processing. *Journal of the American Oil Chemists' Society* 73, 1627–1633.
- Py, X., Guillot, A., Cagnon, B., 2003. Activated carbon porosity tailoring by cyclic sorption/decomposition of molecular oxygen. *Carbon* 41 (8), 1533–1543.
- Rajendran, S., Sai Bharadwaj, A.V.S.L., Barmavatu, P., Palani, G., Trilaksanna, H., Kannan, K., Meenakshisundaram, N., 2024. A review on lanthanum-based materials for phosphate removal. *ChemEngineering* 8 (1), 23.

- Ravikovitch, P.I., Neimark, A.V., 2006. Density functional theory model of adsorption deformation. *Langmuir* 22 (26), 10864–10868.
- Rodríguez-Reinoso, F., Garrido, J., Martín-Martínez, J.M., Molina-Sabio, M., Torregrosa, R., 1989. The combined use of different approaches in the characterization of microporous carbons. *Carbon* 27 (1), 23–32.
- Roth, W.J., Gil, B., Makowski, W., Marszałek, B., Eliášová, P., 2016. Layer like porous materials with hierarchical structure. *Chem. Soc. Rev.* 45 (12), 3400–3438.
- Rouquerol, J., Rouquerol, F., Grillet, Y., Denoyel, R., 1989. The role of thermal analysis and calorimetry in the study of porous or divided materials. *Thermochim Acta* 148, 183–190.
- Rouquerol, J., Llewellyn, P., Rouquerol, F.J.S.S.S.C., 2007. Is the BET Equation Applicable to Microporous Adsorbents? Vol. 160, 49–56.
- Ryu, Z., Zheng, J., Wang, M., Zhang, B., 2000. Nitrogen adsorption studies of PAN-based activated carbon fibers prepared by different activation methods. *J. Colloid Interface Sci.* 230 (2), 312–319.
- Schulte-Herbrüggen, H.M., Semiao, A.J., Chaurand, P., Graham, M.C., 2016. Effect of pH and pressure on uranium removal from drinking water using NF/RO membranes. *Environ. Sci. Tech.* 50 (11), 5817–5824.
- Seifi, A., Bahramian, A.R., Sharif, A., 2016. Correlation between structure and oxidation behavior of carbon aerogels. *J. Storage Mater.* 7, 195–203.
- Sha, Y.H., Hu, N., Wang, Y.D., Chen, S.Y., Zou, C., Dai, Z.R., Ding, D.X., 2019. Enhanced phytoremediation of uranium contaminated soil by artificially constructed plant community plots. *J. Environ. Radioact.* 208, 106036.
- Shah, P.U., Raval, N.P., Vekariya, M., Wadhvani, P.M., Shah, N.K., 2016. Adsorption of lead (II) ions onto novel cassava starch 5-choloromethyl-8-hydroxyquinoline polymer from an aqueous medium. *Water Sci. Technol.* 74 (4), 943–956.
- Shapiro, A.J., O'Dea, R.M., Epps III, T.H., 2023. Thermogravimetric analysis as a high-throughput lignocellulosic biomass characterization method. *ACS Sustain. Chem. Eng.* 11 (49), 17216–17223.
- Sonobe, T., Pipatmanomai, S., Worasuwannarak, N., 2006. Pyrolysis characteristics of Thai-agricultural residues of rice straw, rice husk, and corncob by TG-MS technique and kinetic analysis. In: *In Proceedings of the 2nd Joint International Conference on "sustainable Energy and Environment (SEE'06)*, pp. 21–23.
- Spirin, E.V., Aleksakhin, R.M., Vlaskin, G.N., Utkin, S.S., 2015. Radiation balance of spent nuclear fuel of a fast reactor and natural uranium. *At. Energ.* 119 (2), 142–148.
- Stoekli, F., Guillot, A., Slassi, A.M., Hugi-Cleary, D., 2002. The comparison of experimental and calculated pore size distributions of activated carbons. *Carbon* 40 (3), 383–388.
- Tapia-Rodríguez, A., Luna-Velasco, A., Field, J.A., Sierra-Alvarez, R., 2010. Anaerobic bioremediation of hexavalent uranium in groundwater by reductive precipitation with methanogenic granular sludge. *Water Res.* 44 (7), 2153–2162.
- Tascón, J.M., (Ed.). 2012. *Novel carbon adsorbents*. Elsevier.
- Thommes, M., Kaneko, K., Neimark, A.V., Olivier, J.P., Rodríguez-Reinoso, F., Rouquerol, J., Sing, K.S., 2015. Physisorption of gases, with special reference to the evaluation of surface area and pore size distribution (IUPAC Technical Report). *Pure Appl. Chem.* 87 (9–10), 1051–1069.
- Torkabad, M.G., Keshtkar, A.R., Safdari, S.J., 2017. Comparison of polyethersulfone and polyamide nanofiltration membranes for uranium removal from aqueous solution. *Prog. Nucl. Energy* 94, 93–100.
- Undabeytia, T., Morillo, E., Maqueda, C., 2002. FTIR study of glyphosate–copper complexes. *J. Agric. Food Chem.* 50 (7), 1918–1921.
- Viet, D.Q., Van Vinh, N., Luong, P.H., Tho, V.D.S., 2015. Thermogravimetric study on rice, corn and sugar cane crop residue. *J. Sustain. Energy Environment* 6, 87–91.
- Wang, S., Wang, J., Lin, S., Li, J., 2019. Public perceptions and acceptance of nuclear energy in China: the role of public knowledge, perceived benefit, perceived risk and public engagement. *Energy Policy* 126, 352–360.
- Weber Jr, W.J., Morris, J.C., 1963. Kinetics of adsorption on carbon from solution. *J. Sanit. Eng. Div.* 89 (2), 31–59.
- Wu, F.C., Tseng, R.L., Juang, R.S., 2005. Comparisons of porous and adsorption properties of carbons activated by steam and KOH. *J. Colloid Interface Sci.* 283 (1), 49–56.
- Xie, G., Shang, X., Liu, R., Hu, J., Liao, S., 2011. Synthesis and characterization of a novel amino modified starch and its adsorption properties for Cd (II) ions from aqueous solution. *Carbohydr. Polym.* 84 (1), 430–438.
- Yakout, S.M., El-Deen, G.S., 2016. Characterization of activated carbon prepared by phosphoric acid activation of olive stones. *Arab. J. Chem.* 9, S1155–S1162.
- Yelatontsev, D., 2023. Production of versatile biosorbent via eco-friendly utilization of non-wood biomass. *Chem. Eng. J.* 451, 138811.
- Zänker, H., Heine, K., Weiss, S., Brendler, V., Husar, R., Bernhard, G., Barkleit, A., 2019. Strong uranium (VI) binding onto bovine milk proteins, selected protein sequences, and model peptides. *Inorg. Chem.* 58 (7), 4173–4189.
- Zhang, C., Ji, Y., Li, C., Zhang, Y., Sun, S., Xu, Y., Wu, C., 2023. The application of biochar for CO₂ capture: influence of biochar preparation and CO₂ capture reactors. *Ind. Eng. Chem. Res.* 62 (42), 17168–17181.
- Zhang, W., Xu, C., Che, X., Wang, T., Willför, S., Li, M., Li, C., 2022. Encapsulating amidoximated nanofibrous aerogels within wood cell tracheids for efficient cascading adsorption of uranium ions. *ACS Nano* 16 (8), 13144–13151.
- Zhao, Z., Liao, L., Xiao, X., Du, N., Lin, Y., 2011. Wireless sensing determination of uranium (IV) based on its inhibitory effect on a catalytic precipitation reaction. *J. Radioanal. Nucl. Chem.* 289, 893–898.
- Zhu, W., Li, Y., Dai, L., Li, J., Li, X., Li, W., Chen, T., 2018. Bioassembly of fungal hyphae/carbon nanotubes composite as a versatile adsorbent for water pollution control. *Chem. Eng. J.* 339, 214–222.
- Zou, C., Xu, Z., Nie, F., Guan, K., Li, J., 2023. Application of hydroxyapatite-modified carbonized rice husk for the adsorption of Cr (VI) from aqueous solution. *J. Mol. Liq.* 371, 121137.